Quantum Drude oscillator model of atoms and molecules: Many-body polarization and dispersion interactions for atomistic simulation

Andrew P. Jones and Jason Crain
School of Physics, The University of Edinburgh, Mayfield Road, Edinburgh EH9 3JZ, United Kingdom

Vlad P. Sokhan*
National Physical Laboratory, Hampton Road, Teddington TW11 0LW, United Kingdom

Troy W. Whitfield
Program in Bioinformatics and Integrative Biology, University of Massachusetts Medical School, Worcester, Massachusetts 01605, USA

Glenn J. Martyna†
IBM T.J. Watson Research Center, P.O. Box 218, Yorktown Heights, New York 10598, USA
(Received 16 March 2012; revised manuscript received 4 December 2012; published 15 April 2013)

Treating both many-body polarization and dispersion interactions is now recognized as a key element in achieving the level of atomistic modeling required to reveal novel physics in complex systems. The quantum Drude oscillator (QDO), a Gaussian-based, coarse grained electronic structure model, captures both many-body polarization and dispersion and has linear scale computational complexity with system size, hence it is a leading candidate next-generation simulation method. Here, we investigate the extent to which the QDO treatment reproduces the desired long-range atomic and molecular properties. We present closed form expressions for leading order polarizabilities and dispersion coefficients and derive invariant (parameter-free) scaling relationships among multipole polarizability and many-body dispersion coefficients that arise due to the Gaussian nature of the model. We show that these "combining rules" hold to within a few percent for noble gas atoms, alkali metals, and simple (first-row hydride) molecules such as water; this is consistent with the surprising success that models with underlying Gaussian statistics often exhibit in physics. We present a diagrammatic Jastrow-type perturbation theory tailored to the QDO model that serves to illustrate the rich types of responses that the QDO approach engenders. QDO models for neon, argon, krypton, and xenon, designed to reproduce gas phase properties, are constructed and their condensed phase properties explored via linear scale diffusion Monte Carlo (DMC) and path integral molecular dynamics (PIMD) simulations. Good agreement with experimental data for structure, cohesive energy, and bulk modulus is found, demonstrating a degree of transferability that cannot be achieved using current empirical models or fully *ab initio* descriptions.

DOI: 10.1103/PhysRevB.87.144103 PACS number(s): 34.20.Cf, 02.70.Ss, 31.15.xk, 67.80.de

I. INTRODUCTION

Many-body polarization and dispersion interactions are fundamental driving forces from which the physics of condensed matter emerges. One classic example is liquid water, where many-body polarization effects substantially enhance the molecular dipole moment from its gas-phase value, contributing to water's high dielectric constant and generally unique physical properties;[1] the importance of polarization in ionic solids and solutions has long been recognized.[2–4] Surface tension is sensitive to many-body dispersion forces,[5] particularly in systems stabilized by dispersion such as hydrophobic aggregates and assemblies.[6,7] Treating these long-range interactions is therefore key to gaining an understanding of complex systems.

Atomistic simulation is an important technique that is used to probe the properties of many-body systems and gain physical insight. However, atomistic modeling is limited by the input description of the interactions, whether from an *ab initio* electronic structure theory such as local density functional theory (LDA),[8,9] or empirical potentials.[2,10,11] As the complexity of the systems of interest has grown, current simple models have been found to be insufficient and the importance of models treating many-body polarization and dispersion interactions accurately and efficiently has correspondingly increased although the critical nature of these forces was acknowledged early in the field's development.[2,3,7]

The Drude oscillator model[12–15] mimics the electronic response of an atom or molecule by replacing the true set of electrons and protons with a single negatively charged light quasiparticle, harmonically bound to a positively charged heavy quasinucleus. Treated classically,[12,16] the model yields many-body dipole polarization. However, treating the model quantum mechanically, the quantum Drude oscillator (QDO), in the spirit of a coarse-grained electronic structure, leads to both many-body multipole polarization and dispersion interactions beyond the dipole approximation; the model can be solved with linear scaling in system size.[17,18] It is therefore of current interest to explore the use of the QDO model as a basis for describing long-range forces in the condensed phase to be applied as part of an empirical force field[17,18] or to supplement electronic structure computations that cannot describe dispersion well, for example using quantum dipole-limit Drude oscillators.[19–24]

In this paper, the ability of the QDO model to treat long-range forces in condensed phase systems is assessed. We first analyze analytically the properties of the model. Since the QDO is based on Gaussian on-site interactions, invariant ratios

of dispersion and polarization response coefficients arise. However, these Gaussian invariants are followed surprisingly well by experimental and theoretical results obtained for atoms and closed-shell molecules indicating that this simple model is powerful. The predictions of the classical Drude oscillator model (CDO), the basis for many polarizable models,[2–4,25–28] are discussed as the $\hbar \to 0$ limit of the QDO. Second, we develop a Jastrow-type diagrammatic expansion method for the QDO in order to discern the higher-order many-body responses predicted by the QDO model. Third, a simple scheme is proposed to fit the QDO model's baseline parameters and the model's predictions are compared to response coefficients of atoms and closed-shell molecules. Last, we discuss the development of empirical potentials based on the QDO approach and apply them to study the condensed phase of several noble gases using linear scale techniques.[17,18]

II. THE QDO MODEL BASICS

The QDO model replaces the "on-site" electron-nucleus Coulomb interaction (within a tight-binding picture of electronic structure theory) with an effective harmonic term and replaces Fermi statistics with Boltzmann statistics as the quantum Drude particles are distinguishable (tethered to sites). The quantum Drude "quasiparticle" (a *drudon*) has charge $-q$, which is balanced by an oppositely charged classical particle, the Drude "nucleus" placed at the center of oscillation. The Drude nucleus and Drude particle interact with other particles via Coulombic forces at long range. Each quantum Drude particle is characterized by three parameters, mass, frequency, and charge, $\{\mu,\omega,q\}$. Exchange repulsion, which is absent by construction from the QDO model, must be incorporated effectively through the introduction of short-range cutoff functions to the Coulomb interaction (regularization) and a nontrivial short-range nuclear-nuclear pair potential at minimum.

Utilizing the QDO model to provide a Born-Oppenheimer surface for the treatment of insulators augmented by Coulomb regularization and pair potentials (or more advanced approaches)[29] to model short-range interactions,[10] may prove to be a powerful approach. Indeed, the goal of this paper is to demonstrate that such an exchange-less model is rich through the presentation of analytical results and studies of exemplar applications; this is distinct from taking a model with exchange symmetry and attempting to solve it neglecting exchange.

The unperturbed QDO Hamiltonian is

$$\hat{H}_0 = \frac{\hbar^2}{2\mu}\nabla_{\mathbf{r}}^2 + \frac{1}{2}\mu\omega^2(\mathbf{r}-\mathbf{R})^2,$$

where the center of oscillation is $\mathbf{R}$ and the solution in spherical polar coordinates is given in Ref. 30. For a system of N QDO's interacting with M fixed point charges, the Hamiltonian is

$$\begin{aligned}\hat{H} = &\sum_{k=1}^{N}\hat{H}_{0k} + \sum_{k=1}^{N}\sum_{j=1}^{M} Q_j q_k\left(\frac{1}{|\mathbf{R}_k-\tilde{\mathbf{R}}_j|} - \frac{1}{|\mathbf{r}_k-\tilde{\mathbf{R}}_j|}\right)\\ &+\frac{1}{2}\sum_{k\neq k'=1}^{N} q_k q_{k'}\left(\frac{1}{|\mathbf{R}_k-\mathbf{R}_{k'}|} + \frac{1}{|\mathbf{r}_k-\mathbf{r}_{k'}|}\right.\\ &\left.-\frac{1}{|\mathbf{r}_k-\mathbf{R}_{k'}|} - \frac{1}{|\mathbf{R}_k-\mathbf{r}_{k'}|}\right)\end{aligned} \tag{1}$$

with $\{Q,\tilde{\mathbf{R}}\}$ the charge and position of the fixed point charges. The regularization of the Coulomb interactions is left for later discussion as this does not affect the asymptotic relations to be given next.

III. ATOMIC POLARIZABILITIES IN THE QUANTUM DRUDE MODEL

A. General formalism

The response of an electrically polarizable atom or molecule in an inhomogeneous static field E can be described through an expansion in induced multipole moments.[31] The induced dipole moment is given by

$$\begin{aligned}\mu_i = &\sum_j \alpha_{ij}E_j + \sum_{jk} A_{ijk}E'_{jk} + \frac{1}{2}\sum_{jk}\beta_{ijk}E_jE_k\\ &+\frac{1}{3}\sum_{jkl}B_{ijkl}E_jE'_{kl} + \frac{1}{6}\sum_{jkl}\gamma_{ijkl}E_jE_kE_l\ldots,\end{aligned}$$

the induced quadrupole moment by

$$\Theta_{ij} = \sum_k A_{kij}E_k + \sum_{kl}C_{ijkl}E'_{kl} + \frac{1}{6}\sum_{k\ell}B_{klij}E_kE_l\ldots,$$

and the induced octupole moment by

$$\Omega_{ijk} = \cdots + \alpha_{3,ijklmn}E''_{lmn}\cdots.$$

Here, E_i, E'_{ij}, E''_{ijk} are components of the applied field and its first and second gradients, respectively.

The response coefficients given above are now described: the linear dipole polarizability is α (which will be denoted as α_1 below). The first two of the nonlinear hyperpolarizabilities are β and γ, whilst $\mathbf{B}$ is the first nonlinear multipole (higher than dipole) hyperpolarizability. The third-rank tensor $\mathbf{A}$ describes the dipole-quadrupole polarizability and determines the dipole response due to a field gradient and the quadrupole response due to the field. $\mathbf{C}$ is the quadrupole polarizability,[31] which we will denote α_2 below. The octupole-octupole polarizability, for which no commonly agreed upon symbol exists to our knowledge, is denoted, here, as α_3. We note that for spherically symmetric (unperturbed) systems, $\beta_{ijk}\equiv 0$ and $A_{ijk}\equiv 0$ and the tensors α_1, γ, B, and C each have one independent component.[32]

B. Polarizabilities of the QDO model

The polarizabilities of the spherically symmetric QDO model of this work can be examined by studying the perturbing effect of a test charge δ placed at a large distance $\tilde{R}$ from the center of oscillation along the z axis [Eq. (1) with $M=1, N=1$]. This perturbation to H_0 can be expressed in spherical polar coordinates whose origin is at the center of the QDO oscillation as

$$\begin{aligned}H'(r,\theta) &= \frac{q\delta}{|\tilde{R}+r|} - \frac{q\delta}{\tilde{R}}\\ &= q\delta\sum_{\ell=1}^{\infty}\left(\frac{r^\ell}{\tilde{R}^{\ell+1}}\right)\left(\frac{4\pi}{2\ell+1}\right)^{1/2}\mathcal{Y}_{\ell 0}(\theta),\end{aligned}$$

with the $\mathcal{Y}_{\ell 0}(\theta)$ the $m = 0$ spherical harmonic functions.[30] Polarizablities arise from second-order perturbation theory, as developed in Supplemental Material,[33,34]

$$E^{(2)} = -\sum_{\ell=1} \frac{e^2 \alpha_\ell}{\tilde{R}^{2\ell+2}},$$
$$\alpha_\ell = \left(\frac{q^2}{\mu\omega^2}\right)\left[\frac{(2\ell-1)!!}{\ell}\right]\left(\frac{\hbar}{2\mu\omega}\right)^{\ell-1}. \quad (2)$$

This defines the dipole polarizability $\alpha_{\rm dip} \equiv \alpha_1$ (DD), the quadrupole polarizability $\alpha_{\rm quad} \equiv \alpha_2$ (QQ), the octupole polarizability $\alpha_{\rm oct} \equiv \alpha_3$ (OO), and so on; the polarizablity tensor of the spherically symmetric QDO model is diagonal, $\alpha_{lml'm'} \to \alpha_l \delta_{ll'} \delta_{mm'}$, as described in Ref. 33. In the classical limit, $\hbar \to 0$, only the dipole polarizability is nonzero:

$$\alpha_{\rm dip} \equiv \alpha_1 = \frac{q^2}{\mu\omega^2}, \quad \alpha_\ell = 0, \quad \forall \ell > 1.$$

Hence the *classical* Drude oscillator (CDO) model formally contains dipole polarization effects only, at this level of perturbation theory.

As described above, some responses are absent as a result of the spherical symmetry of the QDO model ($\beta_{ijk} \equiv 0$ and $A_{ijk} \equiv 0$, for instance). Hyperpolarizabilities, which couple even orders of a homogeneous field, such as γ (DDDD), the second hyperpolarizability, are also absent because the model contains no anharmonicity.[33] The model does possess multipole hyperpolarizabilities, starting with the dipole-dipole-quadrupole hyperpolarization $B = 3q^3/(2\mu^2\omega^4)$ (see Ref. 33). Note, B is a classical quantity, independent of $\hbar$, and thus is reproduced within the CDO. Later, we will develop a diagrammatic method based on the Jastrow approach[35] that allows an intuitive understanding of the type of responses that are present/absent in the QDO model.

C. Polarizability invariants of the QDO model

The quantum Drude oscillator model is based on Gaussian on-site interactions. Due to this Gaussian nature, simple relationships amongst the response coefficients arise, that is, Gaussians only possess one independent moment. The first three polarizabilities of the QDO model can be written as

$$\alpha_{\rm dip} \equiv \alpha_1 = \frac{q^2}{\mu\omega^2}, \quad (3a)$$
$$\alpha_{\rm quad} \equiv \alpha_2 = \frac{3}{4}\left(\frac{\hbar}{\mu\omega}\right)\alpha_1, \quad (3b)$$
$$\alpha_{\rm oct} \equiv \alpha_3 = \frac{5}{4}\left(\frac{\hbar}{\mu\omega}\right)^2 \alpha_1 . \quad (3c)$$

From this form, the following invariant emerges:

$$\gamma_{\rm pol} \equiv \frac{2\sqrt{5}\,\alpha_2}{3\sqrt{\alpha_1\alpha_3}} = 1, \quad \forall \text{ QDO},$$

which holds for all quantum Drude models; it is an invariant of the model. Note that the quantity $(\frac{\hbar}{2\mu\omega})$ is the spatial variance of the quantum Drude quasiparticle (that is, the width of the unperturbed QDO's Gaussian ground-state wave function squared).

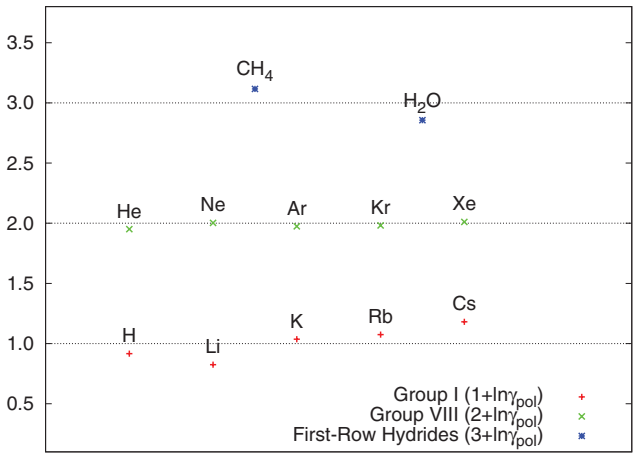

FIG. 1. (Color online) QDO model invariant polarizability scaling relation $\gamma_{\rm pol}$ for three classes of atoms and molecules: alkali-metal atoms (group I), noble gases (group VIII), and small molecules (first-row hydrides). All three classes show good agreement with the QDO prediction, the horizontal lines in the figure, especially the noble gases. The $\gamma_{\rm pol}$ for the three classes are offset for clarity as indicated in the legend/insert.

In assessing the approximations inherent in the QDO model, it is important to determine to what extent $\gamma_{\rm pol}$ is preserved for atoms and molecules. We have selected a test suite of systems, which includes the noble gases, the alkali metals, and the first row hydrides. The latter are reasonably close to spherical in shape and we have used the isotropic part of the molecular polarizability tensors to make the comparison; a single QDO again has spherical symmetry. Figure 1 (and Ref. 33) shows the results of the tests. The quantity $\ln(\gamma_{\rm pol})$ is presented because the relationship is multiplicative and could equally well be inverted. Agreement with the QDO invariant is surprisingly good. For more complex molecules, one would not expect a single QDO to be a good representation; however, we posit, encouraged by the distributed electric multipole and polarizablility based approach,[31,36] that a model with several quantum Drude particles, each representing a molecular moiety, would give a good description of real systems (i.e. with distributed electric multipoles as well as point charges used to describe a moiety's fixed charge distribution and a set of QDO's not necessarily centered on atomic sites to describe its response to external perturbation).

IV. DISPERSION IN THE QUANTUM DRUDE MODEL

The standard dispersion energy between two atoms A and B separated by a distance $R_{\rm AB}$,

$$E_{\rm disp} = -\sum_{n=6,8,10,\ldots} C_n^{\rm AB} / R_{\rm AB}^n, \quad (4)$$

arises from a second-order perturbation theory treatment of electronic structure.[31] The coefficient C_6 captures induced-dipole–induced-dipole fluctuation interactions, C_8 captures induced-dipole–induced-quadrupole interactions, and C_{10} captures induced-dipole–induced-octupole plus induced-quadrupole–induced-quadrupole interactions. There are further two-body interactions, which arise in a third-order in perturbation theory[37] beginning at $\mathcal{O}(R_{\rm AB}^{-11})$. For *nonspherical*

molecules, there exist also terms with odd powers in R_{AB} starting at $\mathcal{O}(R_{AB}^{-7})$. For nearly spherical molecules such as the first-row hydrides (for example, the water molecule),[38] these terms make small contributions. At the three-body level, the leading interaction between spherically symmetric moieties A, B, and C is the Axilrod-Teller-Muto[39] dispersion interaction:

$$E_{3\text{disp}} = C_9^{ABC} \times \frac{3\cos a \cos b \cos c + 1}{R_{AB}^3 R_{AC}^3 R_{BC}^3}$$

(where a is the angle formed at vertex A, and so on).

The QDO model has been used to develop a basic understanding of dispersion[13,31] as it allows the dispersion coefficients to be calculated in closed form.[40] In Ref. 33, we present a derivation of $C_n^{AB}, n = 6,8,10$ starting from Eq. (1) with $M = 0, N = 2$ following Ref. 31. We obtain

$$\begin{aligned} C_6^{AB} &= \frac{3}{2}\alpha_1^A\alpha_1^B\frac{\hbar\omega_A\omega_B}{(\omega_A+\omega_B)}, \\ C_8^{AB} &= \frac{15}{2}\left[\alpha_1^A\alpha_2^B\frac{\hbar\omega_A\omega_B}{(\omega_A+2\omega_B)} + \alpha_2^A\alpha_1^B\frac{\hbar\omega_A\omega_B}{(2\omega_A+\omega_B)}\right], \\ C_{10}^{AB} &= \left[21\alpha_1^A\alpha_3^B\frac{\hbar\omega_A\omega_B}{(\omega_A+3\omega_B)} + 21\alpha_3^A\alpha_1^B\frac{\hbar\omega_A\omega_B}{(3\omega_A+\omega_B)}\right. \\ &\quad \left. + 70\alpha_2^A\alpha_2^B\frac{\hbar\omega_A\omega_B}{(2\omega_A+2\omega_B)}\right], \end{aligned} \tag{5}$$

in agreement with Ref. 40. If the Drude particles are of identical species, $\omega_A = \omega_B = \omega$, $\alpha^A = \alpha^B = \alpha$, then

$$\begin{aligned} C_6^{AA} &= \tfrac{3}{4}\alpha_1\alpha_1\hbar\omega, \quad C_8^{AA} = 5\alpha_1\alpha_2\hbar\omega, \\ C_{10}^{AA} &= \left(\tfrac{21}{2}\alpha_1\alpha_3 + \tfrac{35}{2}\alpha_2\alpha_2\right)\hbar\omega. \end{aligned} \tag{6}$$

It is possible to evaluate three-body dispersion coefficients (such as Axilrod-Teller-Muto triple induced dipole dispersion term)[39] using spherical polar coordinates and Clebsch-Gordan coefficients following Stone.[31] However, we can also use the diagrammatic approach developed below to yield

$$\begin{aligned} C_9^{ABC} &= \frac{1}{2}\alpha_1^A\alpha_1^B\alpha_1^C\frac{\hbar\omega_A\omega_B\omega_C(\omega_A+\omega_B+\omega_C)}{(\omega_A+\omega_B)(\omega_B+\omega_C)(\omega_A+\omega_C)}, \\ C_9^{AAA} &= \frac{3}{16}\alpha_1^3\hbar\omega, \end{aligned}$$

as given in Appendix B. The one component limit agrees with that presented for the one component dipole limit QDO model studied in Ref. 41.

A. Dispersion coefficient invariants of the QDO model

As was the case with the polarizabilities, the Gaussian nature of the QDO model leads to invariant relationships amongst the dispersion coefficients. The four single-species dispersion terms can be simplified as follows:

$$\begin{aligned} C_6 &= \frac{3}{4}\alpha_1\alpha_1\hbar\omega, \quad C_8 = 5\left(\frac{\hbar}{\mu\omega}\right)C_6, \\ C_{10} &= \frac{245}{8}\left(\frac{\hbar}{\mu\omega}\right)^2 C_6, \quad C_9 = \frac{1}{4}\alpha_1 C_6, \end{aligned} \tag{7}$$

where the response coefficients for interacting QDO's of identical species are written as $C_n^{AA} \to C_n$, $C_9^{AAA} \to C_9$. These relationships lead to the identical species two-body scaling law:

$$\gamma_{\text{disp}} \equiv \frac{7}{2\sqrt{10}}\frac{C_8}{\sqrt{C_6 C_{10}}} = 1 \quad \forall\ \text{QDO}, \tag{8}$$

the three-body dispersion invariant relationship

$$\gamma_{3\text{disp}} \equiv \frac{\alpha_1 C_6}{4C_9} = 1 \quad \forall\ \text{QDO}, \tag{9}$$

and the nonidentical species dispersion relation

$$\begin{aligned} \gamma_{\text{mix}} &\equiv \left(\frac{3}{2}\alpha_1^A\alpha_1^B\frac{\omega_A\omega_B}{\omega_A+\omega_B}\right)\Big/ C_6^{AB} \\ &= \left(\frac{C_6^{AA}}{\alpha^A\alpha^A} + \frac{C_6^{BB}}{\alpha^B\alpha^B}\right)\Big/\left(2\frac{C_6^{AB}}{\alpha^A\alpha^B}\right) = 1 \quad \forall\text{QDO}, \end{aligned} \tag{10}$$

where

$$\hbar\omega_s \equiv \frac{4}{3}\frac{C_6^{ss}}{\left(\alpha_1^s\right)^2} \quad (s \in \{A,B\}). \tag{11}$$

The above result is similar to the empirical combining rule of Moelwyn-Hughes.[42,43] Finally, the three-body nonidentical species dispersion scaling relation is

$$\begin{aligned} \gamma_{3\text{mix}} &\equiv \left[\frac{\alpha_1^A\alpha_1^B\alpha_1^C}{C_9^{ABC}}\right]\left[\frac{\hbar\omega_A\omega_B\omega_C(\omega_A+\omega_B+\omega_C)}{(\omega_A+\omega_B)(\omega_B+\omega_C)(\omega_A+\omega_C)}\right] \\ &= 1 \quad \forall\ \text{QDO}, \end{aligned} \tag{12}$$

which is closely related to the empirical combining rule of Refs. 44,45.

The degree to which the QDO dispersion invariants given above describe real systems is assessed in Fig. 2, where $\ln(\gamma_{\text{disp}})$ is given for our selected set of atoms and molecules (see also Ref. 33). The invariant holds rather well. The QDO model three-body dispersion scaling law seems to define a rough upper bound for atoms and simple molecules, $\ln(\gamma_{3\text{disp}}) \geqslant 0$ as shown in Fig. 3 (see also Ref. 33). Figures 4 and 5 demonstrate that the QDO model mixed dispersion coefficient invariant also holds well. In summary, the QDO model shows promise to be simply transferable to complex systems, capturing not just the many-body induction but also

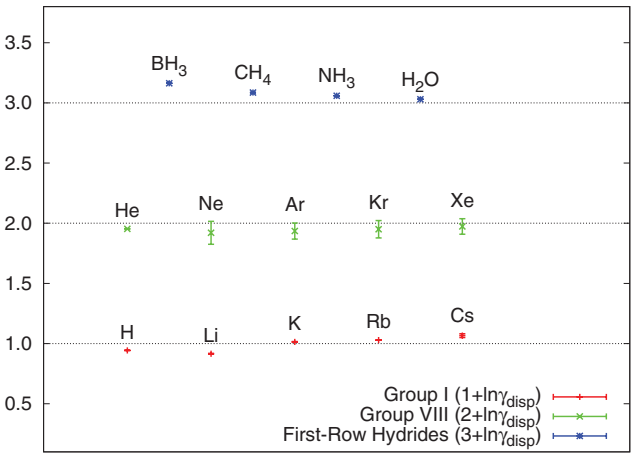

FIG. 2. (Color online) QDO model invariant two-body dispersion scaling relation γ_{disp} for the same three classes of atoms and molecules as in Fig. 1. All satisfy the relation quite closely.

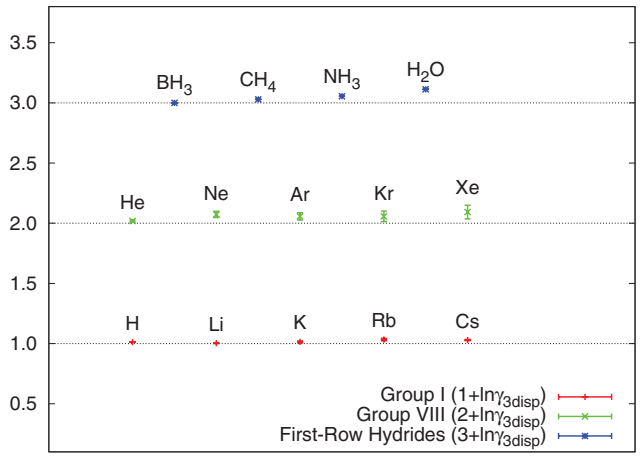

FIG. 3. (Color online) QDO model invariant three-body dispersion scaling relation $\gamma_{3\text{disp}}$ for the same three classes of atoms and molecules as in Fig. 1. All obey the relation quite closely. This time notice that all the values are above the line; it appears there is a systematic tendency for the QDO model to overestimate the value of C_9, but to a very modest degree.

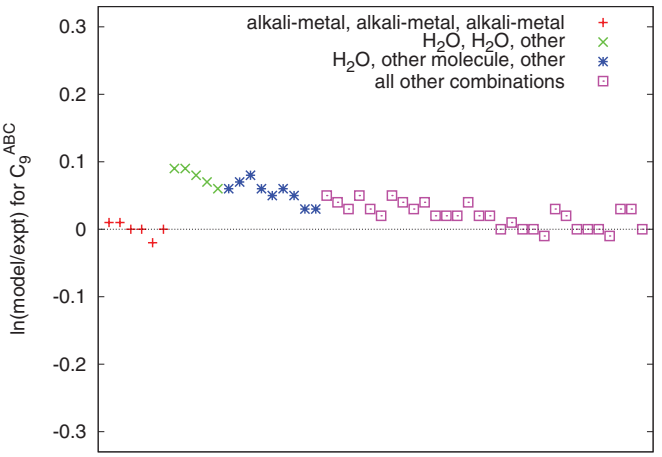

FIG. 5. (Color online) QDO model invariant mixed-species three-body dispersion scaling relation $\gamma_{3\text{mix}}$ for different combinations of atoms and molecules. As in Fig. 3, the model appears to have a small systematic tendency to overestimate C_9, but the prediction is still remarkably close. It is worth bearing in mind that the three-body dispersion is a small energy and it is difficult to measure C_9 directly.

many-body dispersion to a reasonable approximation, even for complex multicomponent assemblies.

V. DISCUSSION OF QDO MODELS AND RELATION TO DIAGRAMMATIC PERTURBATION THEORY

The QDO approach has been shown to give a good description of the low-order dispersion and polarization response coefficients for an important set of atoms and molecules. In order to make further progress in assessing the capabilities of the model, we have developed a Jastrow-type diagrammatic framework[35,46–50] the details of which are given in Appendix A. The diagrammatic framework reveals (a) the responses that must vanish by symmetry, (b) the structure of the responses in terms of $\hbar$ and perturbation theory order, (c) that dispersion arises as loops by analogy with the bubble diagrams of particle physics, and (d) the plethora of responses including cross interactions between polarization and dispersion that the model engenders. Although the QDO is a simplified or coarse grained electronic structure, within the underlying approximations, it contains long-range responses to all orders.

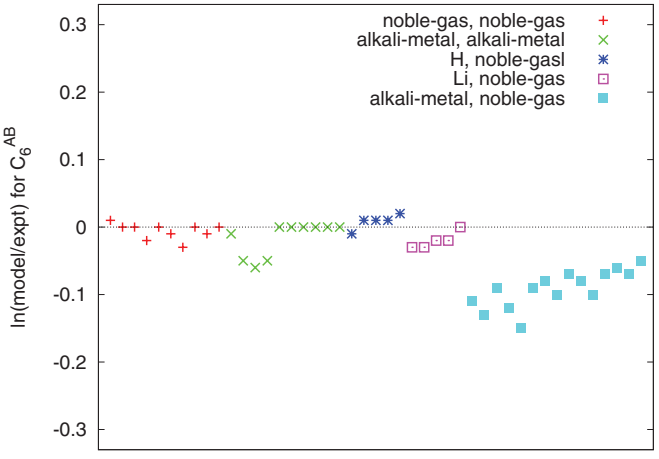

FIG. 4. (Color online) QDO model-invariant mixed-species two-body dispersion scaling relation γ_{mix} for combinations of noble-gas and alkali-metal atoms. The interactions predicted between similar species are more accurate than those between unlike species, but those are also quite close. Alkali atoms are unusual species, which behave quite differently to closed-shell species as reflected in the model parameters in Table I.

The major response classes of our diagrammatic expansion are shown Fig. 7; the diagrams that exist in the dipole limit are given in Fig. 8. They can be interpreted intuitively given the following guide (illustrated in Fig. 6). Each (yellow) box represents an instance of the electrostatic potential between two particles (one at either end), which can be written as a multipole expansion.[31] Multiple (yellow) boxes thus indicate successive levels in perturbation theory. That is, a single (yellow) box indicates energies that appear at first order—the straightforward electrostatic interaction. Two (yellow) boxes connected at only one end represent the interaction between fields at a particular particle, specifically, the interaction of a field with the multipole-moment induced by the same or another field—this is the polarization (an energy term that arises from second-order perturbation theory).[31] Three (yellow) boxes connected at one junction therefore represent hyperpolarization (third order).[31] Four such boxes represent second hyperpolarization (fourth order) and so on.

Diagrams where all ends of the (yellow) boxes are connected (no free ends) indicate terms which exist even when there are no permanent fields present (that is, there are no fields at first order). These are pure dispersion/van der Waals energies, which start at second order (see Fig. 8 for the dispersion diagrams in the dipole limit). Note that these terms form loops (akin to "bubble diagrams" in particle physics, where they contribute to the self-energy of the quantum field except that in this case, the quantum field is made up of discrete QDO's at variable locations rather than a lattice representing a continuous field). Note that many-body polarization (involving permanent fields, but more than one junction), many-body

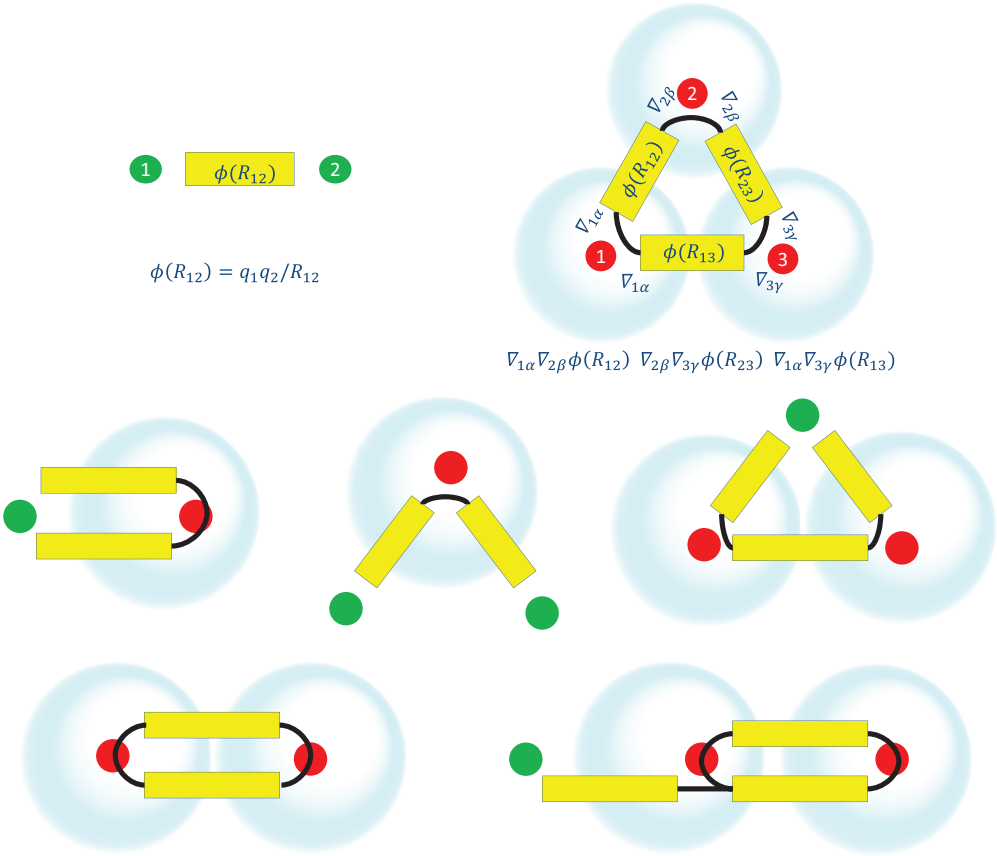

FIG. 6. (Color online) Selected diagrams (yellow and black) interpreted in terms of QDO's (blue cloud, red centers) and charges (green). A shift of the center of the blue cloud indicates polarization. Dispersion does not show such shifts in mean-field atomic representations like this, but does appear as loops in the diagrams. For the yellow and black diagrams, a yellow bar indicates a primitive electronic multipole interaction $Q_{\ell m} T_{\ell m \ell' m'} Q_{\ell' m'}$.[31] The number of thin black lines coming out of one end of a yellow bar indicates ℓ, the kind of multipole (0 = monopole, 1 = dipole, 2 = quadrupole, and so on) involved at that particle in the interaction. The diagrams show, in order, the simple Coulomb potential between two charges, three-body dispersion, simple two-body polarization, polarization at a single center, many-body polarization, two-body dispersion, and polarization dispersion. Mathematical expressions corresponding to elements of the diagrams are also shown for the first two diagrams (omitting prefactors for clarity).

dispersion (loops with more than two junctions), and even polarization-dispersion interactions (permanent fields and loops) are all described as well. The connectors indicate tensor inner products of multipole field gradients. The multiplicity of line ends at the end of a box indicate which multipole is involved in that interaction. A single line at the end of box indicates a dipole, double lines indicate a quadrupole, and so on. Figure 6 illustrates how the diagrams imply interactions between QDO's and an external Coulomb field.

One important property of the diagrammatic perturbation theory presented here is that it allows classification and interpretation of the terms generated (i.e., the QDO model is sufficiently simple that the perturbation theory neatly exposes long-range intermolecular forces). The column in which a diagram is situated indicates at which order it appears in perturbation theory, and the row indicates the power in $\hbar$ of the interaction. Thus only the top row ($\hbar^0$) of interactions exist for the classical Drude oscillator. The first column of Fig. 7 represents the regular Coulomb potential between fixed point charges. The second column diagrams represent, in order, dipole-dipole polarization, quadrupole-quadrupole polarization, dipole-dipole dispersion, octupole-octupole polarization, quadrupole-quadrupole dispersion, and dipole-octupole dispersion—all of them the result of second-order perturbation theory. The third column contains third-order effects, and so on.

It can be seen that higher order responses do indeed exist within the QDO model. For example, the leading-order cross interactions (third column, second row, middle 2) occur when the dipole-dipole dispersion interacts with dipole- and quadrupole polarizations, respectively. There is also a dipole-dipole-quadrupole polarization energy (third column, first row, bottom), and two corresponding dispersion terms (dispersion-only diagrams, third column, third row, rightmost 2), indicating that QDO's have a nonzero dipole-dipole-quadrupole hyperpolarizability, which we calculate in Appendix A.

It is important to note that using the Jastrow diagrammatic approach it is possible to determine easily that certain interactions must be absent. For example, there is no diagram for three-dipole or four-dipole hyperpolarization (no diagrams with 3 or 4 single lines joined around the same junction—more discussion is given in Appendix A). The ability of this framework to determine which higher order responses exist

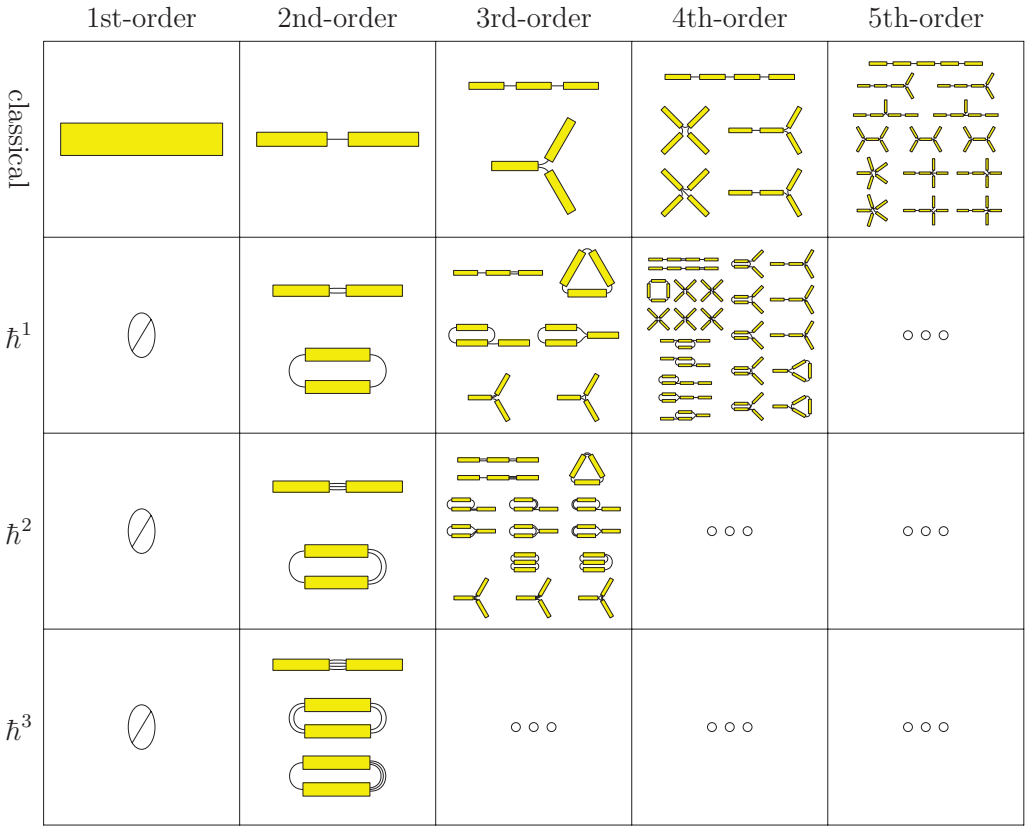

FIG. 7. (Color online) Full diagrammatic expansion of QDO interactions. First, see Fig. 6 for explanation of the individual diagrams. The column number, also the number of yellow bars, is the order at which each term would appear in Rayleigh-Schrödinger perturbation theory. The row number is the power in $\hbar$: the top row is $\hbar^0$ and shows all the interactions that are possible with a CDO (classical limit), where the leading terms involve dipole polarization, although there are some others, including the dipole-dipole-quadrupole polarizability. The QDO has all rows, bringing both higher-multipole interactions (multiple black lines) and dispersion (closed loops).

could become useful as the systems to which the QDO model is applied become more advanced. We point out that the simplicity of the QDO model (distinguishable quasiparticles), allows the simplified perturbation theory to achieve a degree of clarity in the study of intermolecular long-range forces[13] but does not approximate well the complete electronic structure problem[46–50] at short-range where exchange repulsion is dominant.

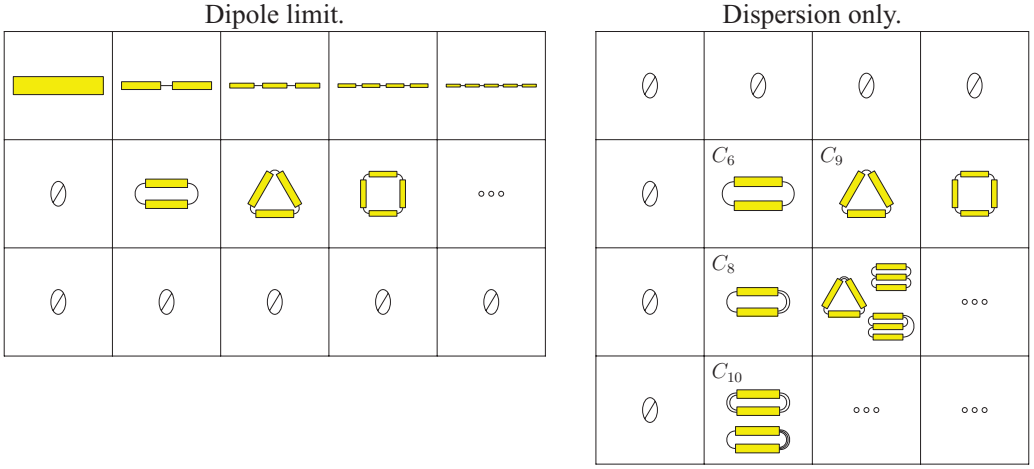

FIG. 8. (Color online) Two subsets of diagrams from Fig. 7. On the left are the terms that exist in the dipole limit: the quantum *dipole* oscillator. These are the subset of terms that can be captured using dipole-limit methods such as matrix diagonalization. Note that a classical *dipole* oscillator would capture only the top row of these; a very limited subset. On the right are the pure dispersion terms. These are the Van der Waals interactions that persist even where there are no charges or fields. Note that there are three-body and four-body (and higher) dispersion terms, and third-order two-body terms.

TABLE I. Quantum Drude parameters determined from C_6, C_8, and α_1.

Species	ω	μ	q
H	0.4273	0.6099	0.7080
Li	0.0687	1.2545	0.9848
K	0.0630	0.8101	0.9670
Rb	0.0603	0.7343	0.9274
Cs	0.0531	0.6939	0.8950
He	1.0187	0.5083	0.8532
Ne	1.2965	0.3491	1.2494
Ar	0.7272	0.3020	1.3314
Kr	0.6359	0.2796	1.3741
Xe	0.5152	0.2541	1.3570
H_2O	0.6287	0.3232	1.1257
NH_3	0.5603	0.3541	1.2722
CH_4	0.5794	0.2615	1.2313
BH_3	0.8776	0.1165	1.0793

VI. PARAMETERIZATION OF QDO MODELS

The closed form expressions that relate the baseline QDO parameters, $\{q,\mu,\omega\}$, to polarizabilities and dispersion coefficients can be rearranged into a form that allows a set of leading order responses to be reproduced exactly. Here, we choose to fix the set $\{\alpha_1, C_6, C_8\}$,

$$\omega = \frac{1}{\hbar}\frac{4C_6}{3\alpha_1^2}, \quad \mu = \frac{\hbar}{\omega}\frac{5C_6}{C_8}, \quad q = -\sqrt{\mu\omega^2\alpha_1}, \qquad (13)$$

although other choices are possible. We take q to be negative as the QDO particle represents a coarse grained electronic structure. QDO parameters determined from Eq. (13) for the atoms and simple molecules in our test set can be found in Table I and are presented graphically in Fig. 9. Interestingly, α_2, α_3, C_{10}, and C_9 (see Tables II–IV) as well as the leading-order dispersion coefficient between unlike species given in Tables V and VI are reproduced well by QDO models parameterized according to Eq. (13).

The QDO parameters selected using the scheme proposed here show a progression within a chemical group but are quite similar to each other (see Fig. 9). It is interesting to note that the effective charge parameter q is clustered around $1e$. The noble gases Ne, Ar, Kr, Xe, seem to be well described using $\omega \approx 0.6$ and $\mu \approx 0.2$; while the alkali atoms Li, K, Rb, Cs can be treated using $\omega \approx 0.06$ and $\mu \approx 0.7$. This difference in behavior is likely due to the fact that noble gases have tightly bound closed shells, whereas alkali-metal atoms have an extra valence electron that forms a loosely bound electronic state [hence the low binding energy $\hbar\omega$ and wide distribution ($\sigma^2 = \hbar/2\mu\omega$), which allows for large polarization effects]. Large polarizabilities in turn produce strong dispersion interactions.[51] Note that the parameters for the first-row hydrides (water, ammonia, methane) are similar to those of the noble gases. In contrast to the group I atoms, the smaller polarizabilities of the first-row hydrides are due to their tightly bound, closed outer electronic shells (like the noble gases). At room temperature, $\hbar\omega/kT \approx 60$ for the alkalis, and $\approx$600 for the others, which indicates that all the model atoms are strongly dominated by the ground-state wave function, as assumed in our analysis.

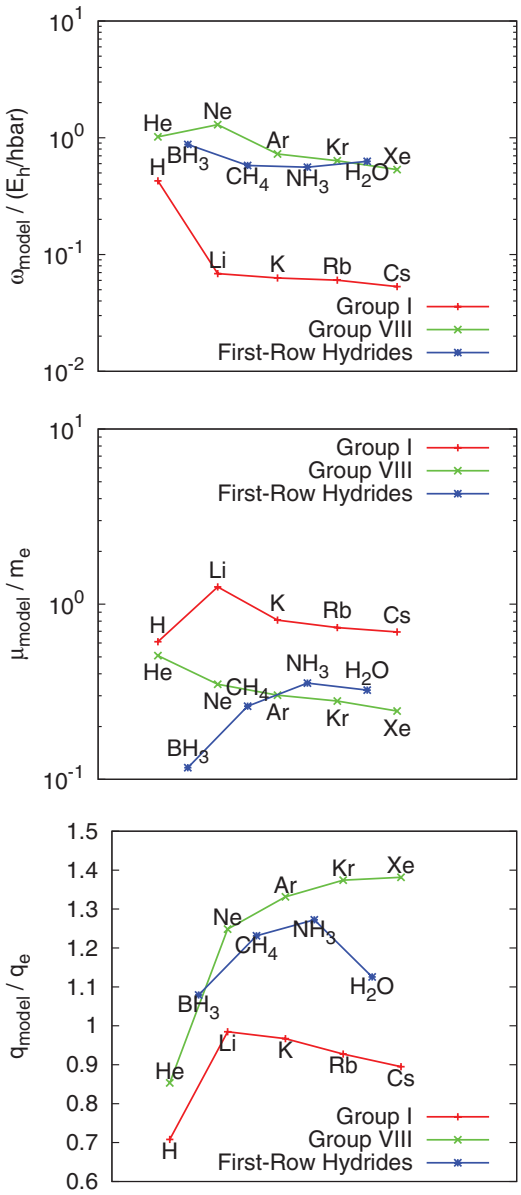

FIG. 9. (Color online) Model parameters $\{\omega,m,q\}$ from fits to C_6, C_8, and α_1, for three classes of atoms and molecules: alkali metal atoms (group I), noble gases (group VIII), and small near-spherical molecules (first-row hydrides). Interestingly, the charge parameter q is about $1e$ and varies the least (note the different y scale). The parameters for noble gases and the small molecules are more similar to each other than to the alkali metal atoms. The difference in parametrization (factor of ten in the ground-state energy $\hbar\omega$) reflects a difference in behavior, which is likely due to the fact that noble gases and small molecules are both closed-shell species, whereas alkali metal atoms have a loosely bound and thus more mobile valence electron, which is also what makes them reactive.

The similarity of QDO parameters for closed-shell first-row hydrides and noble gas atoms suggests that if the QDO model can treat the condensed phase properties of noble gases (as has already been shown to be the case for xenon),[18,52] it will also yield a good description of other unreactive species, including molecular groups such as methyls, amines, hydroxyls, and even ions (at least non-transition-metal ions). It is worth noting

TABLE II. Quantum Drude model polarizabilities.

Species	α_1/a_0^3	α_2/a_0^5			α_3/a_0^7		
	model (=expt)	model	expt	$\ln\left(\frac{\text{model}}{\text{expt}}\right)$	model	expt	$\ln\left(\frac{\text{model}}{\text{expt}}\right)$
H	4.5	12.95	15	−0.15	82.8	131.3	−0.46
Li	164	1428	1383	0.03	2.76×10^4	3.68×10^4	−0.29
K	291	4277	4597	−0.07	1.40×10^5	1.50×10^5	−0.07
Rb	322	5453	5979	−0.09	2.05×10^5	2.13×10^5	−0.04
Cs	409	8321	9478	−0.13	3.76×10^5	3.40×10^5	0.10
He	1.38	2.00	2.44	−0.20	6.43	10.6	−0.50
Ne	2.66	4.41	6.42	−0.38	16.25	34.27	−0.75
Ar	11.1	37.91	50.21	−0.28	287.7	531.3	−0.61
Kr	16.7	70.44	95.55	−0.30	660	1260	−0.65
Xe	27.3	156.4	212.6	−0.31	1991	3602	−0.59
H_2O	9.92	36.61	32.37	0.12	300.3	313.2	−0.04
NH_3	14.56	55.04	88.08	−0.47	462.3	–	–
CH_4	17.27	85.5	104.8	−0.20	940	1121	−0.18
BH_3	12.98	95.2	. . .	. . .	1552	. . .	. . .

that group I *atoms* are radicals, highly reactive species that we do not expect to model with the nonreactive QDO approach beyond the present study of long-range asymptotic responses.

VII. QDO-BASED MODELS FOR NEON, ARGON, KRYPTON, AND XENON

Here, we describe the development of QDO models for the noble gases. In Ref. 52, a QDO model of xenon was fit using experimental data for the polarizabilities and dispersion coefficients, as above, to determine the three principal model parameters $\{\mu,\omega,q\}$ via Eq. (13), and then was augmented with Coulomb regularization and a short-range internuclear pairwise repulsion potential. Here, we develop the QDO models for neon, argon, and krypton using the same approach. We then apply the models to determine the ground-state properties of their solid phases using linear-scale NC-DMC method[18] and the thermodynamic properties of their liquid phase at state points related by the classical law of corresponding states via a linear-scale PIMD simulation.[17] The aim of this exercise is to assess the transferability and applicability of the QDO approach to simple systems in addition to xenon.

A. Fitting QDO models: long-range asymptotics

Using Eq. (13) of Sec. VI, the principal QDO parameters $\{\mu,\omega,q\}$ for Ne, Ar, Kr, and Xe, were fit to reproduce the desired set of corresponding leading order response coefficients, $\{C_6,C_8,\alpha_1\}$ (see Tables I and II). Short-range Coulomb regularization and classical pair potentials are described next.

B. Short-range damping of Coulomb interactions in the QDO model

Drudons are distinguishable quasiparticles obeying Boltzmann statistics whose purpose is to describe accurately the long-range response of atoms or molecular groups. Since Fermi statistics are neglected, a short-range empirical damping of the model's Coulomb interactions are introduced to mimic this effect. It is not clear what functional form this Coulomb regularization should take. In Ref. 52, the simple potential

TABLE III. Quantum Drude model dispersion coefficients.

Species	$C_6/E_h a_0^6$			$C_8/E_h a_0^8$		
	model	expt	$\ln\left(\frac{\text{model}}{\text{expt}}\right)$	model	expt	$\ln\left(\frac{\text{model}}{\text{expt}}\right)$
H	6.49	6.47–6.51	(−0.003)–(+0.003)	124.5	124.0–125.0	(−0.00)–(+0.00)
Li	1385	1380–1390	(−0.004)–(+0.004)	8.04×10^4	$7.89–8.19 \times 10^4$	(−0.02)–(+0.02)
K	4000	3970–4030	(−0.007)–(+0.008)	3.92×10^5	$3.84–4.00 \times 10^5$	(−0.02)–(+0.02)
Rb	4690	4640–4740	(−0.011)–(+0.011)	5.30×10^5	$5.16–5.43 \times 10^5$	(−0.03)–(+0.03)
Cs	6665	6630–6700	(−0.005)–(+0.005)	9.040×10^5	$8.58–9.50 \times 10^5$	(−0.05)–(+0.05)
He	1.46	1.44–1.47	(−0.010)–(+0.010)	14.05	13.9–14.2	(−0.01)–(+0.01)
Ne	6.88	6.48–7.27	(−0.056)–(+0.059)	76.0	55.5–96.5	(−0.24)–(+0.31)
Ar	67.2	63.6–70.8	(−0.052)–(+0.055)	1530	1180–1880	(−0.21)–(+0.26)
Kr	133	124–142	(−0.065)–(+0.070)	3740	2940–4540	(−0.19)–(+0.24)
Xe	298.5	272–325	(−0.085)–(+0.093)	1.14×10^4	8900–13900	(−0.20)–(+0.25)
H_2O	46.4	46.4	(0.00)	1142	1142	(0.00)
NH_3	89.08	89.08	(0.00)	2245	2245	(0.00)
CH_4	129.6	129.6	(0.00)	4277	4277	(0.00)
BH_3	110.9	110.9	(0.00)	5423	5423	(0.00)

TABLE IV. Quantum Drude model dispersion coefficients (continued)

Species	$C_{10}/E_h a_0^{10}$ model	$C_{10}/E_h a_0^{10}$ expt	$\ln\left(\frac{\text{model}}{\text{expt}}\right)$	$C_9/E_h a_0^9$ model	$C_9/E_h a_0^9$ expt	$\ln\left(\frac{\text{model}}{\text{expt}}\right)$
H	2926	3270–3290	(−0.12)–(−0.11)	7.3	7.2–7.22	(+0.01)
Li	5.72×10^6	$6.50–7.05 \times 10^6$	(−0.21)–(−0.13)	5.68×10^4	5.66×10^4	(+0.00)
K	4.71×10^7	$4.40–4.76 \times 10^7$	(−0.01)–(+0.07)	2.91×10^5	2.87×10^5	(+0.01)
Rb	7.32×10^7	$6.64–7.18 \times 10^7$	(+0.02)–(+0.10)	3.78×10^5	3.65×10^5	(+0.03)
Cs	1.50×10^8	$1.23–1.40 \times 10^8$	(+0.07)–(+0.20)	6.81×10^5	6.62×10^5	(+0.03)
He	166.2	181–184	(−0.10)–(−0.09)	0.50	0.49–0.49	(+0.02)–(+0.02)
Ne	1029	826–1520	(−0.39)–(+0.22)	4.57	4.11–4.38	(+0.04)–(+0.11)
Ar	4.27×10^4	$3.49–6.09 \times 10^4$	(−0.36)–(+0.20)	186.5	172–180	(+0.04)–(+0.08)
Kr	1.29×10^5	$1.09–1.70 \times 10^5$	(−0.28)–(+0.17)	555.3	511–536	(+0.04)–(+0.08)
Xe	5.33×10^5	$4.28–6.75 \times 10^5$	(−0.24)–(+0.22)	2037	1790–1910	(+0.06)–(+0.13)
H_2O	3.44×10^4	3.24×10^4	(+0.06)	115.07	102.73	(+0.11)
NH_3	6.93×10^4	6.16×10^4	(+0.12)	324.25	306.87	(+0.06)
CH_4	1.73×10^5	1.46×10^5	(+0.17)	559.55	543.67	(+0.03)
BH_3	3.25×10^5	2.35×10^5	(+0.33)	359.87	...	...

form

$$\phi_{xy}(r) = q_x q_y \left[1 - \exp\left(-r^4/\gamma_{xy}^4\right)\right]/r \tag{14}$$

was suggested, where x and y stands for Drude particle d or nucleus n, as appropriate. The convenient choice of Ref. 52 is not claimed to be optimal or unique but goes to zero at $r = 0$ and to unity in the limit r goes to infinity.

TABLE V. Comparison of model and experimental dispersion coefficients between unlike species.

Species A	Species B	$C_6^{AB}/E_h a_0^6$ model	$C_6^{AB}/E_h a_0^6$ expt.	Δ ln
He	Ne	3.140	3.120	0.01
He	Ar	9.748	9.720	0.00
He	Kr	13.53	13.60	−0.01
He	Xe	19.80	20.10	−0.01
Ne	Ar	20.63	20.70	−0.00
Ne	Kr	28.41	28.70	−0.01
Ne	Xe	41.20	42.30	−0.03
Ar	Kr	94.30	94.30	−0.00
Ar	Xe	140.0	141.0	−0.01
Kr	Xe	198.5	199.0	−0.00
H	Li	65.46	66.30	−0.01
H	K	107.8	113.0	−0.05
H	Rb	114.9	122.0	−0.06
H	Cs	130.6	137.0	−0.05
Li	K	2348	2350	−0.00
Li	Rb	2542	2540	0.00
Li	Cs	3013	3020	−0.00
K	Rb	4330	4330	−0.00
K	Cs	5146	5150	−0.00
Rb	Cs	5586	5575	0.00
H	He	2.804	2.820	−0.01
H	Ne	5.771	5.710	0.01
H	Ar	20.17	20.00	0.01
H	Kr	28.81	28.50	0.01
H	Xe	43.76	42.90	0.02

Since the QDO model of xenon constructed in Ref. 52 performed reasonably well, we adopt Eq. (14) here. Rather than refit the $\{\gamma\}$ for each noble gas, the values for the xenon model of Ref. 52 were assumed to be "universal" and scaled in proportion to the corresponding LJ diameters denoted L; for example, $\{\gamma^{(Ne)}\} \equiv (L_{Ne}/L_{Xe})\{\gamma^{(Xe)}\}$. Values are given in Table VII.

C. Short-range classical pair-wise repulsion

Elegant QDO models containing only short-range Coulomb regularization could, in principle, be developed. However, this has been difficult to realize in practice whilst keeping

TABLE VI. Comparison of model and experimental dispersion coefficients between unlike species (cont.).

Species A	Species B	$C_6^{AB}/E_h a_0^6$ model	$C_6^{AB}/E_h a_0^6$ expt.	Δ ln
He	Li	21.82	22.50	−0.03
He	K	35.71	39.80	−0.11
He	Rb	37.96	43.20	−0.13
He	Cs	42.77	46.80	−0.09
Ne	Li	42.64	43.90	−0.03
Ne	K	69.72	78.90	−0.12
Ne	Rb	74.07	86.10	−0.15
Ne	Cs	83.33	91.60	−0.09
Ar	Li	171.2	174.0	−0.02
Ar	K	280.8	305.0	−0.08
Ar	Rb	298.7	331.0	−0.10
Ar	Cs	337.4	362.0	−0.07
Kr	Li	254.3	259.0	−0.02
Kr	K	417.4	451.0	−0.08
Kr	Rb	444.3	489.0	−0.10
Kr	Cs	502.4	538.0	−0.07
Xe	Li	408.4	408.0	0.00
Xe	K	671.3	709.0	−0.05
Xe	Rb	715.0	769.0	−0.07
Xe	Cs	810.0	850.0	−0.05

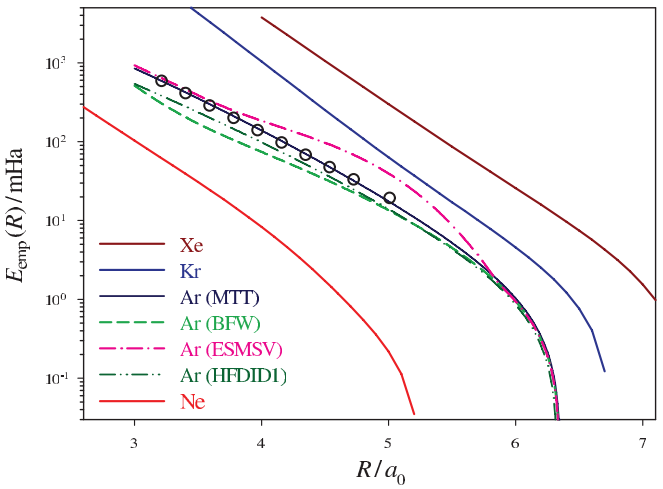

FIG. 10. (Color online) Repulsive wall of selected empirical potentials. From top to bottom, the curves are BWSLS potentials for xenon (X2) and krypton (K2);[54] composite ESMSV,[57] MTT,[56] HFDID1,[58] and BFW[53] for argon; ESMSV potential for neon.[55] Circles are the experimental data as cited in Ref. 56.

simple (practical) functional forms and fitting procedures. Therefore a "classical" pair-wise repulsion interaction $V_{rep}(r)$ acting between the Drude centers is added to the QDO model, following the basic tenants outlined in Ref. 10. One way to determine such a "repulsive wall" is to calculate the Born-Oppenheimer (BO) surface of the regularized QDO model dimer using NC-DMC simulations,[18] and then to compare the result with a high-quality empirical gas phase pair potential. The required short-range "classical" pair potential can be defined to be the difference between these two functions such that the QDO model reproduces properties built into the gas phase pair potential in the low-density limit. We chose to fit the difference data to a triexponential form following Ref. 52,

$$V_{rep}(r) = \sum_{i=1}^{3} \kappa_i \exp(-r/\lambda_i), \tag{15}$$

which is not unique or presumed optimal but is sufficiently flexible to fit the data.

For noble gases, there are a number of accurate gas phase empirical pair-potentials described in the literature, broadly based on the (SCF) Hartree–Fock/dispersion decomposition.[10] The BWSLS potential was selected for use in the krypton and xenon cases.[54] For neon, we employed the potential of Ref. 55 as our baseline. Finally, for argon, we used the potential of Ref. 56. The short-range repulsive parts of the considered potentials are compared in Fig. 10. Several argon potentials are presented in the figure for comparison. These choices of baseline empirical potential are based on convenience and not on extensive testing.

Using the principal QDO parameters, $\{\mu,\omega,q\}$, presented in Table I, the regularization presented, above, and the NC-DMC[18] method, we calculated the BO surface of the regularized QDO model for each (isolated) noble gas dimer at 20–25 internuclear separations in the range between $0.5L$ and $2L$. This range covers the potential well and the repulsive wall (L is the Lennard-Jones diameter often denoted σ). In the NC-DMC calculations, we used $N_w = 200$ walkers and an imaginary time step of $\hbar\tau\omega = 0.01$. In a typical run, after the initial equilibration of 5×10^4 steps, the energy was averaged over further 10^6 steps. We next fit the triexponential function of Eq. (15) to the difference between the empirical potential and the calculated QDO energy surface. The parameters of the short-range pair potentials determined using this approach are given in Table VII. The QDO energies with their fitted pair repulsion included (symbols) are compared in Figs. 11–13 to the empirical potentials (full line); the results obtained at short range are given as insets.

TABLE VII. Parameters for the quantum Drude model of several noble gases. All quantities are in atomic units, unless stated otherwise.

	Ne	Ar	Kr	Xe[a]
L (nm)	0.26743	0.3405	0.368	0.4055
κ_1 (MHa)	265.447	26.6754	6.98489	60.1475
κ_2 (MHa)	761.389	21.5104	26.0932	63.8244
κ_3 (MHa)	−1026.76	−48.1804	−33.0672	−123.961
λ_1 (bohr^{-1})	3.117951	1.059684	1.914719	1.7033100
λ_2 (bohr^{-1})	3.111181	2.250861	1.924938	1.6995777
λ_3 (bohr^{-1})	3.112895	4.280202	1.922674	1.7013642
ϵ_{surf}	1.52	1.90	2.27	2.85

[a]Short-range repulsion parameters for Xe are different from published previously.[52]

D. Fitting QDO models: beyond the noble gases

In the previous sections, we have described a simple procedure to fit QDO models for the noble gases based on principles described in pioneering work on intermolecular forces.[2,10,32] Many-body, long-range interactions were introduced with suitable cutoffs within the QDO model, and short-range interactions subsequently added. Historically, short-range interactions have been fit to a combination of

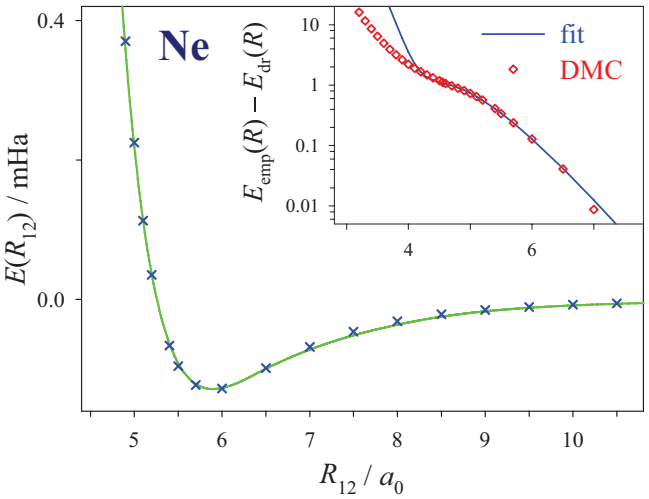

FIG. 11. (Color online) Fitting the short-range repulsion for neon. Full line is the ESMSV potential,[55] crosses are the NC-DMC results plus triexponential fit. On the inset: diamonds are the difference between the ESMSV potential and the results of the damped NC-DMC calculation, full line is a triexponential fit.

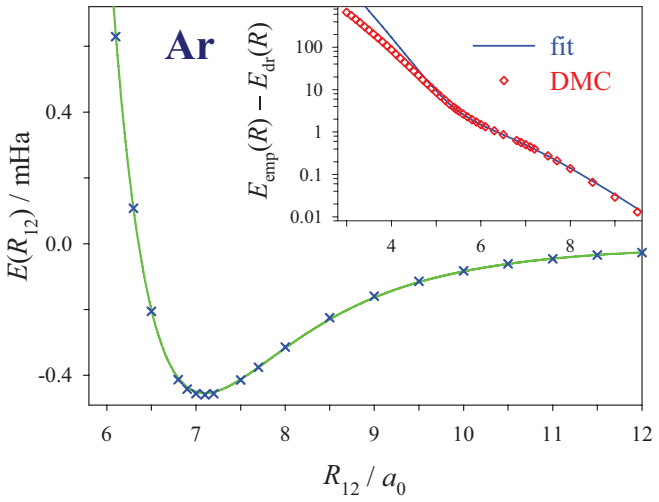

FIG. 12. (Color online) The same as in Fig. 11, only for argon using the MTT potential.[56]

quantum-mechanical computations and experimental data. This basic approach has also been applied to develop models of water[25] and alkali halides,[2] for instance. It should be noted that a "perfect" pair potential (from perhaps a coupled cluster or a even full CI computation) would fail to predict condensed phase systems if pertinent many-body effects are not taken into account as demonstrated by Barker[7] for the noble gases, for example. More recently, a technique has been developed to limit the error associated with fitting (short-range interactions) to insufficiently flexible functional forms.[29]

In order to develop accurate force fields to treat molecular systems, or molecular moieties, more advanced approaches have been proposed. Stone has pioneered the use of distributed multipoles to describe the charge distribution of *ab initio* computations[31,59] and others have developed techniques to place polarizable sites in such system from *ab initio* input.[36] The baseline model for long-range interactions is often taken to be the CDO (i.e., plus electrostatics). At present, van der Waals interactions are added as two-body terms with coefficients

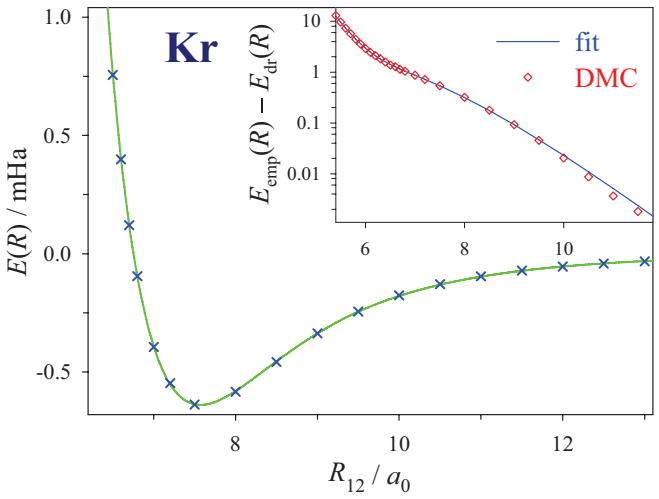

FIG. 13. (Color online) The same as in Fig. 11, only for krypton using the BWLSL (K2) potential.[54]

taken either from experiment or computed from quantum chemistry. Based on the results presented here, it would seem natural and plausible to replace the CDO with the QDO in order to potentially generate more powerful and accurate models (note, using gas phase, two-body, van der Waals coefficients can lead to an error in the condensed phase predictions if three-body terms are neglected).[7]

It has been a "holy grail" to develop a fully *ab initio* approach for potential function generation. Three exemplar papers in this area are Refs. 11,27,28, which rely on CDO's. These approaches follow the basic outline of the previous paragraph as regards long-range interactions and as stated above, replacing the CDO's of these models with QDO's would be an interesting research endeavor. The precise methodology used to partition the energy from fully *ab initio* computations, while interesting and important, is beyond the current, more narrow, discussion.

Lastly, the full QDO model could be used to correct local density functional theory computations following the work using the dipole limit QDO[19–23] or to augment mixed approaches such as the effective fragment model.[60] However, the solution to the full model is more difficult than the dipole limit and such a combined approach would require development. Success would allow bond making and breaking processes to be explored, i.e., a reactive force field with an improved treatment of long-range interactions.

E. Scaling of the QDO approach with system size

Using the adiabatic path integral molecular dynamics method to simulate the QDO model,[17,52] the computational complexity of a QDO calculation scales as N, where N is the number of atoms in the system. The $\mathcal{O}(N)$ scaling arises because in the discrete path integral picture of quantum statistical mechanics[61] under the Boltzmann statistics appropriate for the QDO model, each classical particle (here each drudon) is replaced by a ring polymer of P beads with each bead representing a time slice of the imaginary time propagator; the number of imaginary time slices, P, is independent of N. The "intrapolymer" interactions are the nearest time slice; bead i of particle j interacts via a harmonic spring with beads $i+1$ and $i-1$ of the same particle j, only, resulting in order N scaling for this portion of computation, i.e., with fixed *prefactor* P. The beads interact via the external potential in a time ordered fashion, that is, only particles of the same bead number i interact with each other via the external potential, which also yields order N scaling, with prefactor P. In periodic systems, the scaling is slightly increased to $N \ln N$ if the Coulomb interactions inherent in the QDO model's external potential are evaluated via particle mesh type methods,[62,63] for instance, or simply N if periodic fast multipole techinques are employed.[64] Since path integral molecular dynamics methods can be efficiently parallelized[65] and very large parallel machines are available, the *prefactor* P can be effectively reduced.

The question of convergence with the sampling time of the method is also important. Our path integral molecular dynamics technique is designed to sample the phase space of a statistical mechanical system at finite temperature using the QDO model to provide an accurate BO surface. Thus the method is order N in the same sense as the standard molecular

TABLE VIII. Comparison of the calculated and experimental zero-temperature properties of noble-gas solids. The quoted energies are per atom.

	Ne	Ar	Kr	Xe
Λ	0.490	0.154	0.0840	0.0522
$E_{\rm calc}(a_0)$ (mHa)	−0.7342	−3.0255	−4.3324	−6.0080
$E_{\rm exp}(a_0)$ (mHa)[a]	−0.6528(16)	−2.948(19)	−4.25(8)	−6.10(8)
$\Delta E_{\rm qc}$ (mHa)	0.233	0.294	0.230	0.204
$a_{\rm calc}$ (Å)	4.4632	5.3154	5.6466	6.1417
$a_{\rm exp}$ (Å)	4.4635	5.3002	5.6458	6.1320
$\Delta a_{\rm qc}$ (Å)[b]	0.1741	0.0635	0.0370	0.0248
$B_{\rm calc}$ (GPa)	0.94(10)	3.11(30)	3.09(20)	3.26(20)
$B_{\rm exp}$ (GPa)	0.99(10)	2.58(15)	3.21(16)	3.65(20)
$\Delta B_{\rm qc}$ (GPa)	0.73	0.49	0.31	0.20

[a]Reference 70.
[b]Reference 71.

dynamics or Monte Carlo techniques. If the statistical mechanical system of interest has a rough energy landscape or is near a phase transition, then the simple order N scaling breaks down for the path integral based QDO technique in the same way as for standard methods. However, many of the phase space sampling acceleration methods that aid standard molecular dynamics and Monte Carlo methods can be applied to enhance sampling in the path integral based QDO model.

F. DMC simulations of noble gas FCC crystals at $T = 0$ K

In order to validate the QDO models for the noble gases presented above, we first test the ability of the models to reproduce the experimentally measured properties of noble gas face centered cubic (FCC) crystals[66] near $T = 0$ K. The NC-DMC method was employed to simulate these perfect crystals in conjunction with the Ewald summation technique to treat the Coulomb interactions. To remove finite size effects, the results were extrapolated to the thermodynamic limit using the appropriate scaling laws; system sizes ranging from $N = 4$ to $N = 500$ atoms were studied. Implementing twist average boundary conditions (k-point sampling)[67] would eliminate the need for the extrapolation at the expense of a more complicated computation.

In order to estimate the bulk ground-state properties of the considered noble gases crystals, including lattice constants, cohesive energies, and bulk moduli, we calculated the total energy for a range of lattice spacings, a, around the experimental result (8–12 points between $0.96a_{\rm exp}$ and $1.04a_{\rm exp}$). The results were fit to the Birch-Murnaghan equation of state.[68] Since the atomic nuclei were treated classically, nuclear quantum corrections[69] need to be applied to make meaningful comparison with experiment. This is accomplished, within first-order perturbation theory, using the nuclear quantum corrections determined in Ref. 69 for Lennard-Jones models of each noble gas crystal as a baseline. For example, we estimate $E_{\rm QDO} \approx E^{\rm (CN)}_{\rm QDO} + (E_{\rm LJ} - E^{\rm (CN)}_{\rm LJ})$, where CN denotes classical nuclei and LJ Lennard-Jones model; the difference is assumed to remove model dependence to first order. The extrapolated results, together with available experimental data are collected in Table VIII; the extrapolations are themselves given graphically in Supplemental Material.[33]

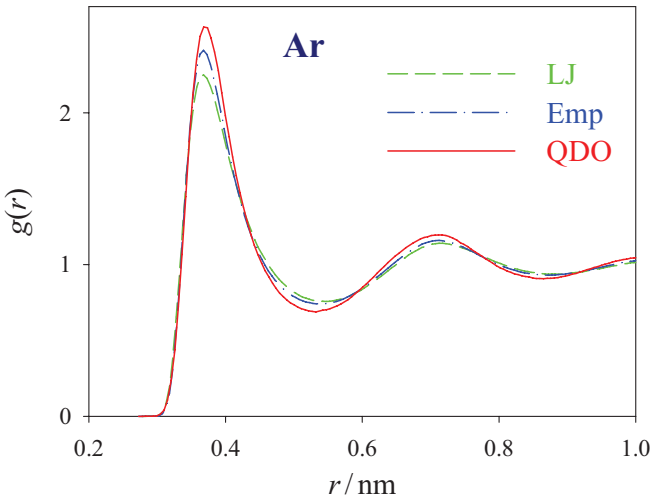

FIG. 14. (Color online) The radial distribution functions for argon calculated using the QDO model via PIMD (red line), the MTT potential[56] (blue dash-dotted line), and the Lennard-Jones model (green dashed line) at the reduced density $\rho^* = 0.7$ and reduced temperature $T^* = 1.25$.

The QDO model lattice parameters show uniformly good agreement with experiment. The QDO model energies also agree well with experiment (<3% deviation for all species except neon, which shows an 8% deviation; this will require future work to understand). QDO model predictions of the bulk modulus agree with experimental measurements within the estimated error bars of experiment and our computations.

G. Liquid phase simulations

In order to assess the ability of QDO model noble gases to describe accurately the liquid phase, we performed a series of finite temperature $P = 80$ bead (Trotter number) PIMD simulations[52] at the thermodynamic state $\rho^* = 0.7$ and $T^* = 1.25$, which lies in the liquid phase of both the generic LJ fluid, and all the physical systems studied here, Ar, Kr, and Xe (i.e., when converted appropriately using the Lennard-Jones parameters of Ref. 69). A convergence study with Trotter number is given in Supplemental Material.[33] The simulated QDO model radial distribution functions for three gases are compared to results produced using the underlying empirical gas phase pair potential and the LJ potential[69] in Figs. 14–16. The slight differences between the models and violations of corresponding states of the QDO model will be explored in future work.

VIII. SUMMARY AND CONCLUSIONS

In this paper, an assessment of the ability of the QDO model to treat the long-range asymptotic behavior of atoms and simple molecules has been performed. Closed form expressions for polarizabilities and dispersion coefficients are presented and invariant scaling relations/combining rules are constructed that reflect the underlying Gaussian nature of the model. We find that the scaling laws are satisfied surprisingly well for (real) atoms and molecules. A diagrammatic perturbation of the Jastrow type is described that demonstrates the (many) allowed responses of this Gaussian-based, exchange-less,

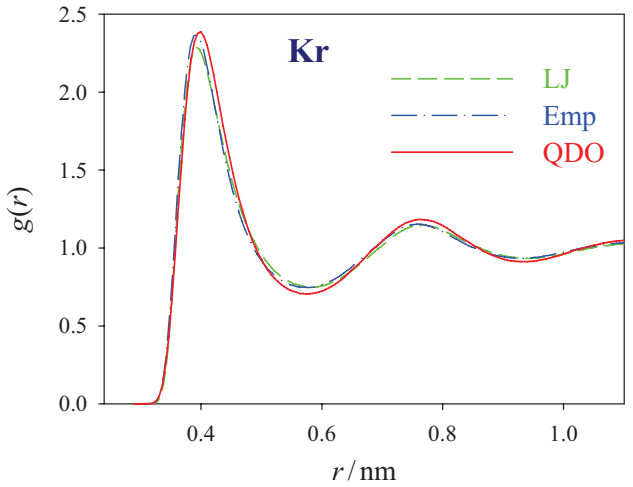

FIG. 15. (Color online) The radial distribution functions for krypton calculated using a QDO model using PIMD (red line), BWLSL (K2) potential[54] (blue dash-dotted line), and Lennard-Jones model (green dashed line) at the reduced density $\rho^* = 0.7$ and reduced temperature $T^* = 1.25$.

approach. This is consistent with the surprising realism that simple models based on Gaussian statistics often exhibit. The QDO model is therefore a strong candidate to serve as a baseline for building long-range forces into atomistic descriptions of complex systems.

We have shown how to parametrize the quantum Drude model $\{q,\mu,\omega\}$ to treat atoms and small molecules using their dipole polarizability α_1, and dominant dispersion coefficients C_6 and C_8, making it possible to create simple models, which yield realistic long-range forces. We discovered that these parameters vary little for closed-shell/unreactive chemical species (noble gases and first-row hydrides), suggesting that other such closed form species (which are the norm in nonreactive molecular dynamics simulations), will also turn out to be well suited to a quantum Drude model based framework. The developed QDO models for neon, argon, krypton, and xenon based on the general principles elucidated in early work on long-range forces[10,32] perform well both for the structural and thermodynamic properties studied here. It will be of interest in the parametrization of more complex systems to use the QDO to perhaps replace the more basic classical Drude oscillator model underlying many current force field models[11,26–28,31,36,59] and/or to enhance the results of *ab initio* computations as in Refs. 19–24.

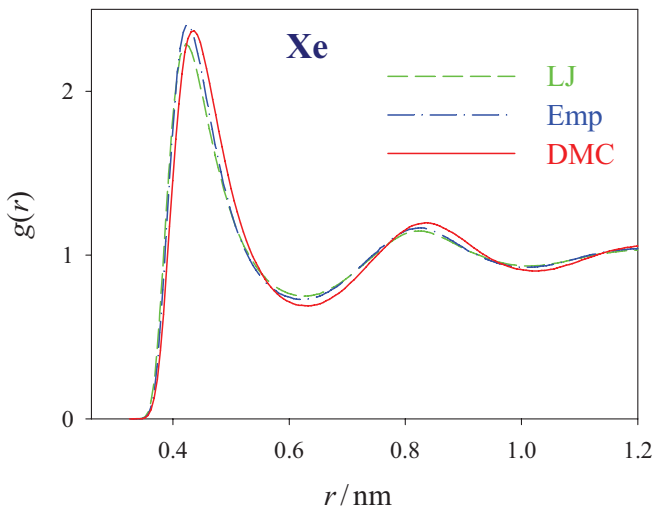

FIG. 16. (Color online) The radial distribution functions for xenon calculated using a QDO model using PIMD (red line), BWLSL (X2) potential[54] (blue dash-dotted line), and Lennard-Jones model (green dashed line) at the reduced density $\rho^* = 0.7$ and reduced temperature $T^* = 1.25$.

ACKNOWLEDGMENTS

J.C. acknowledges support from EPSRC and the National Physical Laboratory. G.J.M. acknowledges support from IBM Research and the University of Edinburgh. A.J. is supported by the National Physical Laboratory. IBM (Blue Gene/L at Watson Research Center) and NPL (Dell PowerEdge workstation) contributed support in the form of computer time. We thank Flaviu Cipcigan, University of Edinburgh, and Dennis M. Newns, IBM Research, for their comments on our work.

APPENDIX A: DIAGRAMMATIC EXPANSION FOR QDO MODELS

We can express the ground-state wave function of a system of interacting QDO's, exactly, as the noninteracting case with a Jastrow-type modification $F(\mathbf{x})$. If the "drudon" coordinates are represented in the vector $\mathbf{x}$ and the potential by $\phi(\mathbf{x})$,

$$\Psi_0(\mathbf{x}) = \exp\left[-\frac{\mu\omega}{2\hbar}\mathbf{x}^2 + F(\mathbf{x})\right] \text{ is our ansatz,}$$

$$\frac{(\hat{H} - E_0)\Psi_0(\mathbf{x})}{\Psi_0(\mathbf{x})} = \phi(\mathbf{x}) - \hbar\omega\mathbf{x}\cdot\nabla F(\mathbf{x}) + \frac{\hbar^2}{2\mu}\nabla F(\mathbf{x})\cdot\nabla F(\mathbf{x}) + \frac{\hbar^2}{2\mu}\nabla^2 F(\mathbf{x}) - E_0.$$

We note that since QDO particles are distinguishable, $\Psi_0(\mathbf{x})$ is positive semidefinite, and the Jastrow factor $F(\mathbf{x})$ is a strictly real function. As the QDO model is spinless, issues of spin-contamination, which arise in the Jastrow-Slater approach to electronic structure, are absent. Hence it is natural to apply the Jastrow approach to the QDO model; the simplicity and yet richness of the QDO approach avoids complexities inherent in the strongly related coupled cluster[46] and Fermi-hypernetted chain[48] approaches to the full electronic structure problem and exposes the physics of long-range forces of interest here as noted in Ref. 13.

If we had the exact closed form expression for $F(\mathbf{x})$, then Eq. (A1) would be solved and both sides would be equal to zero. However, we can also solve it iteratively. The natural first perturbation is (following Ref. 18) the one that cancels the first two terms in the RHS:

$$\phi(\mathbf{x}) - \hbar\omega\mathbf{x}\cdot\nabla F(\mathbf{x}) = 0.$$

If $\phi(\mathbf{x})$ and $F(\mathbf{x})$ are expressed as a multipole expansion, then each term is a simple polynomial $\phi_\ell(\mathbf{x})$, making $F_\ell(\mathbf{x})$ simple to find; it is of the same form but possesses a different prefactor. For example, $F_\ell(\mathbf{x}) = \frac{1}{\ell\hbar\omega}\phi_\ell(\mathbf{x})$. Clearly, terms with $\ell = 0$, which means terms like x^0, cannot be canceled in this

way. They are constant terms such as $\phi(0)$ that do not vary in space and are canceled by adding them to the ground-state energy E_0 instead.

We can go further. Using the perturbation generated by the first cancellation, the third and fourth terms on the right-hand side of Eq. (A1) are now remainder terms:

$$\frac{\hbar^2}{2\mu}\left[\nabla F(\mathbf{x})\right]^2 = \frac{1}{2\ell^2\mu\omega^2}\left[\nabla\phi(\mathbf{x})\right]^2,$$
$$\frac{\hbar^2}{2\mu}\nabla^2 F(\mathbf{x}) = \frac{\hbar}{2\ell\mu\omega}\nabla^2\phi(\mathbf{x}),$$

(for the Coulomb potential, $\nabla^2\phi=0$, but there are important higher order perturbations that are constructed in this way but are nonzero). These remainder terms can be canceled in turn by a second round of perturbations added to $F(\mathbf{x})$. As the leftover terms are also polynomials, the cancellation perturbation again is of the same form, with only a different prefactor. The new perturbations yield new remainder terms, which can in turn be canceled by a third round of perturbations to $F(\mathbf{x})$, and so on. Although evaluating these expressions in closed form can be complex, the *form* of each term is relatively simple to write down, and this gives us insight into the *types* of interactions that are present. This is precisely the goal of a diagrammatic theory.

It is convenient to label the terms with two subscripts n and m: n is the number of instances of the bare potential ϕ (or its fields/gradients), which appear in the interaction. It is equivalent to the corresponding level in Rayleigh-Schrödinger perturbation theory. Higher levels in n are generated by $[\nabla F]\cdot[\nabla F]$-type operations, involving new interactions between existing fields and terms. m is the power in $\hbar$, the "level of quantumness" of the interaction. Higher levels in m are generated by $\nabla^2 F$ operations, involving the divergence of existing fields or terms. New terms created from the diagrammatic energy expansion in Fig. 7 were generated by the following iteration neglecting the multipole factors ℓ:

$$G_{n,m}(\mathbf{x}) = \frac{\hbar^2}{2\mu}\sum_{\nu=1}^{n-1}\sum_{\mu=0}^{m}[\nabla F_{\nu,\mu}]\cdot[\nabla F_{n-\nu,m-\mu}] \quad \text{(from terms left and above left)}$$
$$+\frac{\hbar^2}{2\mu}\nabla^2 F_{n,m-1} \quad \text{(from terms above)},$$
$$F_{n,m}(\mathbf{x}) \approx \frac{1}{\hbar\omega}\left[G_{n,m}(\mathbf{x}) - G_{n,m}(0)\right] \quad \text{(ignore } \ell\text{)},$$
$$E_{n,m} = G_{n,m}(0).$$

Note that the two kinds of terms bring different factors: each time a new F term is generated, it brings a factor of $1/\hbar\omega$, but every time the divergence operator is applied it brings a factor $\hbar^2/2\mu$. If we continue to ignore ℓ,

$$[\nabla F]\cdot[\nabla F] \Rightarrow \frac{\hbar^2}{2\mu}\left(\frac{1}{\hbar\omega}\right)^2 = \frac{1}{\mu\omega^2} = \frac{\alpha}{q^2},$$
$$\nabla^2 F \Rightarrow \frac{\hbar^2}{2\mu}\left(\frac{1}{\hbar\omega}\right)^2 = \frac{\alpha}{q^2}\hbar\omega \qquad \text{(a new factor of } \hbar\text{)}.$$

The contributions to the energy $E_{n,m}$ are constant terms, and they do not contribute to further iterations of the wave-function perturbation. They sum together to form the ground-state energy E_0. Diagrams belonging to $E_{n,m}$ may be found in the column n (also the number of yellow boxes), row m of Fig. 7. n is also the number of yellow boxes in the diagram, and m is also the number of inner products (black connectors), more than the bare minimum required to join the boxes together.

A (yellow) box represents the Coulomb potential. On its own it represents that the portion of the energy that is independent of the QDO parameters (depending only on any permanent multipole moments of the molecule). The interaction potential is always between two particles, so the boxes are drawn long. A line end coming out one end of a (yellow) box represents the potential's first (vector) derivative at that particle, which is a dipole field. Two line ends at one box end represent the potential's second derivative at that particle, a quadrupole field. Two such line ends joined represent a tensor dot product (summation over an index) between two such fields, an interaction, at a particular QDO particle (thus the lines must be short):

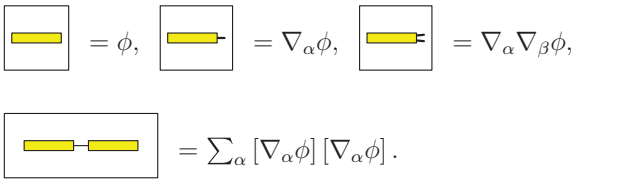

The subsequent energy terms derived via $[\nabla F]\cdot[\nabla F]$ operation involve joining two existing diagrams with a new line to form a new diagram. The line represents an interaction between the fields and a particle at a particular point, so these connector lines are all drawn short. This also constrains which interaction diagrams are "legal:".

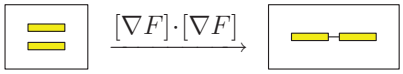

TABLE IX. Polarizability elements for various symmetries.[32]

Symmetry	Number of independent elements					
	$\alpha_{\alpha\beta}$	$\beta_{\alpha\beta\gamma}$	$\gamma_{\alpha\beta\gamma\delta}$	$A_{\alpha,\beta\gamma}$	$B_{\alpha\beta,\gamma\delta}$	$C_{\alpha\beta,\gamma\delta}$
Sphere	1	0	1	0	1	1
$D_{\infty h}$	2	0	3	0	4	3
C_{2v}	3	3	6	4	9	6
C_1	6	10	15	15	30	15

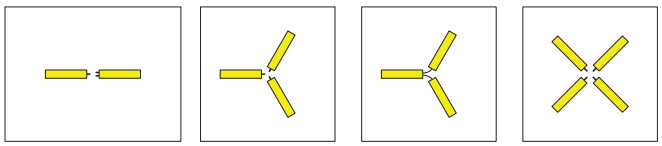

(a) $A_{\alpha\beta\gamma}$ dipole-quadrupole polarization is absent.

(b) $\beta_{\alpha\beta\gamma}$ 3-dipole hyperpolarization is absent.

(c) $B_{\alpha\beta\gamma\delta}$ 2-dipole-quadrupole hyperpolarization is present.

(d) $\gamma_{\alpha\beta\gamma\delta}$ 4-dipole hyperpolarization is absent.

FIG. 17. (Color online) Allowed/forbidden interaction-diagrams: interactions that are allowed by the QDO model can easily be determined by checking if it is possible to join the requisite parts with black lines and no loose ends. Loose ends would indicate derivative tensors; energies must be scalars.

The terms created via $\nabla^2 F$ add a new connector to an existing diagram to form a new diagram (along with a power in $\hbar$). This can create loops, which represent dispersion terms (akin to "bubble diagrams" as described in the text), or parallel connectors, which indicate (further) derivatives of the Coulombic field, i.e., multipoles. That is, single connectors represent dipole interactions, double connectors represent quadrupole interactions, and triple connectors represent octupole interactions:

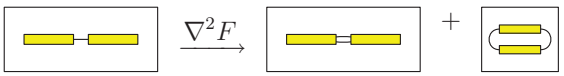

A single QDO has spherical symmetry. As given in Table IX, it can therefore has only a few independent components in its polarizability tensors and some tensors vanish entirely. For example, the dipole-quadrupole polarizability $A_{\alpha\beta\gamma}$ and the three-dipole hyperpolarizability $\beta_{\alpha\beta\gamma}$ are both forbidden by symmetry, while the two-dipole-quadrupole hyperpolarization and the four-dipole hyperpolarizability tensors each have one independent component. Figure 17 shows that our diagrammatic technique correctly predicts that $A_{\alpha\beta\gamma}$ and $\beta_{\alpha\beta\gamma}$ vanish (by symmetry) but also correctly predicts that the four-dipole hyperpolarizability is forbidden by the Gaussian nature of the QDO (see also Ref. 33). If a four-dipole hyperpolarizability tensor is desired, then on-site anharmonic interactions must be added to the QDO model. We also note that more than one QDO can be placed in a molecular frame to break spherical symmetry if desired. We leave these intriguing possibilities for future work.

APPENDIX B: THREE-BODY DISPERSION (IN THE DIPOLE LIMIT)

In Appendix A, we split the potential $\phi(\mathbf{x})$ into polynomials of order ℓ and solve F_ℓ for each ϕ_ℓ:

$$\mathbf{x}\cdot\nabla F_\ell(\mathbf{x}) = \ell\, F_\ell(\mathbf{x}) = \phi_\ell(x) \quad \Rightarrow \quad F_\ell(\mathbf{x}) = \frac{\phi_\ell(\mathbf{x})}{\hbar\ell\omega},$$

but we wish to build the wave function for a combination of QDO's with an arbitrary set of parameters. This means that ω are not all identical. In this case, it is makes sense to split the potential $\phi(\mathbf{x})$ into contributions $\phi_{ij\ldots}(x_i, x_j, \ldots)$ and then further split these into $\phi_{ij\ldots,\ell\ell'\ldots}$ of order ℓ in x_i, ℓ' in x_j etc., so that we can solve $F_{ij,\ell\ell'\ldots}$ for each $\phi_{ij,\ell\ell'\ldots}$. For example, for a two-body potential, where i and j are particle indices:

$$\phi_{ij,\ell\ell'}(\mathbf{x}) = \frac{1}{\ell!\ell'!}\, x_i^\ell T_{ij}^{(\ell+\ell')} x_j^{\ell'},$$

where $T_{ij}^{(\ell+\ell')} \equiv \nabla^{(\ell)}\nabla^{(\ell')}(1/R_{ij})$ is a tensor of rank $(\ell+\ell')$, we have

$$\left(\hbar\omega_i\, x_i\frac{\partial}{\partial x_i} + \hbar\omega_j\, x_j\frac{\partial}{\partial x_j}\right)\; F_{ij,\ell\ell'}(\mathbf{x}) = \hbar\left(\ell\omega_i + \ell'\omega_j\right)\; F_{ij,\ell\ell'}(\mathbf{x}) = \phi_{ij,\ell\ell'}(\mathbf{x}),$$

which gives

$$F_{ij,\ell\ell'}(\mathbf{x}) = \frac{\phi_{ij,\ell\ell'}(\mathbf{x})}{\hbar(\ell\omega_i + \ell'\omega_j)}.$$

If we restrict the calculation to the dipole limit, that means $\ell = \ell' = 1$, and all expressions are quadratic with two indices in x, and therefore relatively simple. Proceeding as before,

$$\begin{aligned}\Psi &\propto \exp\left[-\frac{\mu\omega}{2\hbar}\mathbf{x}^2 - \textstyle\sum_{n=1}^N F^{(n)}(\mathbf{x})\right],\\ &\quad\times \sum_{ij}\left[\hbar\omega_i\, x_i\frac{\partial F^{(n)}(\mathbf{x})}{\partial x_i} + \hbar\omega_j\, x_j\frac{\partial F^{(n)}(\mathbf{x})}{\partial x_j}\right]\\ &\equiv G^{(n-1)}(\mathbf{x}) - G^{(n-1)}(0),\end{aligned}$$

where

$$G^{(0)}(\mathbf{x}) = \phi(\mathbf{x}) = \frac{1}{2}\sum_{ij} q_i q_j x_i T_{ij} x_j$$

is the physical potential and higher terms are

$$\begin{aligned}G^{(1)}(\mathbf{x}) &= -\frac{\hbar^2}{2\mu}\nabla F^{(1)}\cdot\nabla F^{(1)} + \frac{\hbar^2}{2\mu}\nabla^2 F^{(1)},\\ G^{(2)}(\mathbf{x}) &= -\frac{\hbar^2}{2\mu}[2\nabla F^{(1)}\cdot\nabla F^{(2)}] + \frac{\hbar^2}{2\mu}\nabla^2 F^{(2)},\\ G^{(3)}(\mathbf{x}) &= -\frac{\hbar^2}{2\mu}[2\nabla F^{(1)}\cdot\nabla F^{(3)} + \nabla F^{(2)}\cdot\nabla F^{(2)}]\\ &\quad + \frac{\hbar^2}{2\mu}\nabla^2 F^{(3)},\end{aligned}$$

and so on.

This yields, in sequence,

$$F^{(1)} = \sum_{ij}\frac{q_i q_j}{\hbar(\omega_i+\omega_j)} x_i T_{ij} x_j\,, \quad G^{(1)} = -\sum_{ijk}\frac{q_i q_j^2 q_k x_i T_{ij} T_{jk} x_k}{2\mu_j(\omega_i+\omega_j)(\omega_j+\omega_k)}, \quad F^{(2)} = -\sum_{ijk}\frac{q_i q_j^2 q_k x_i T_{ij} T_{jk} x_k}{2\mu_j\hbar(\omega_i+\omega_j)(\omega_j+\omega_k)(\omega_i+\omega_k)},$$

$$G^{(2)} = -\frac{\hbar}{8}\sum_{ij}\left(\frac{q_i^2}{\mu_i\omega_i^2}\right)\left(\frac{q_j^2}{\mu_j\omega_j^2}\right)\frac{\omega_i\omega_j}{\omega_i+\omega_j} T_{ij}T_{ji} \qquad \leftarrow \text{two-body dispersion}$$

$$-\sum_{ijk\ell}\frac{q_i q_j^2 q_k^2 q_\ell x_i T_{ij} T_{jk} T_{k\ell} x_\ell}{\mu_i\mu_j(\omega_i+\omega_j)(\omega_j+\omega_k)(\omega_i+\omega_k)(\omega_k+\omega_\ell)},$$

$$F^{(3)} = -\sum_{ijk\ell}\frac{q_i q_j^2 q_k^2 q_\ell x_i T_{ij} T_{jk} T_{k\ell} x_\ell}{\mu_i\mu_j\hbar(\omega_i+\omega_j)(\omega_j+\omega_k)(\omega_i+\omega_k)(\omega_k+\omega_\ell)(\omega_i+\omega_\ell)},$$

$$G^{(3)} = -\sum_{ijk}\frac{\hbar\, q_i^2 q_j^2 q_k^2 T_{ij} T_{jk} T_{k\ell}}{\mu_i\mu_j\mu_k(\omega_i+\omega_j)(\omega_j+\omega_k)(\omega_i+\omega_k)(\omega_k+\omega_i)(2\omega_i)} + \mathcal{O}(x^2, T^4).$$

The first term of $G^{(3)}$ is the three-body dispersion. We can symmetrize it in the indices i,j,k, yielding

$$G^{(3)} = -\frac{\hbar}{24}\sum_{ijk}\left(\frac{q_i^2}{\mu_i\omega_i^2}\right)\left(\frac{q_j^2}{\mu_j\omega_j^2}\right)\left(\frac{q_k^2}{\mu_k\omega_k^2}\right)\frac{\omega_i\omega_j\omega_k(\omega_i+\omega_j+\omega_k)}{(\omega_i+\omega_j)(\omega_j+\omega_k)(\omega_i+\omega_k)}T_{ij}T_{jk}T_{ik}\,.$$

Evaluating the T tensors leads to

$$G^{(3)} = -\frac{\hbar}{8}\sum_{ijk}\frac{\alpha_{1i}\alpha_{1j}\alpha_{1k}\,\omega_i\omega_j\omega_k(\omega_i+\omega_j+\omega_k)}{(\omega_i+\omega_j)(\omega_j+\omega_k)(\omega_i+\omega_k)}\frac{\left[3\cos(i\hat{j}k)\cos(j\hat{k}i)\cos(k\hat{i}j)+1\right]}{R_{ij}^3R_{jk}^3R_{ik}^3}.$$

The sum can be rearranged to remove double counting, which elucidates the total contribution from each triple:

$$-\frac{\hbar}{8}\sum_{ijk}\to-\frac{(3!)\hbar}{8}\sum_{i>j>k}=-\frac{3\hbar}{4}\sum_{i>j>k}.$$

---

*Part of this work was carried out while on a secondment to IBM Watson Research Centre.

†martyna@us.ibm.com

[1] Edited by F. Franks, *Water a Comprehensive Treatise: The Physics and Physical Chemistry of Water*, Vol. I (Plenum Press, New York, 1972).

[2] W. Cochran, Philos. Mag. **4**, 1082 (1959).

[3] M. Sangster and M. Dixon, Adv. Phys. **3**, 247 (1976).

[4] M. Wilson, P. A. Madden, M. Hemmati, and C. A. Angell, Phys. Rev. Lett. **77**, 4023 (1996).

[5] J. Miyazaki, J. A. Barker, and G. M. Pound, J. Chem. Phys. **64**, 3364 (1976).

[6] I. R. McDonald and L. V. Woodcock, J. Phys. C **3**, 722 (1970).

[7] J. A. Barker, Phys. Rev. Lett. **57**, 230 (1986).

[8] P. Hohenberg and W. Kohn, Phys. Rev. **136**, B864 (1964).

[9] W. Kohn and L. Sham, Phys. Rev. **140**, A1133 (1965).

[10] V. P. S. Nain, R. A. Aziz, P. C. Jain, and S. C. Saxena, J. Chem. Phys. **65**, 3242 (1976).

[11] J. Antony, J.-P. Piquemal, and N. J. Gresh, J. Comp. Chem. **26**, 1131 (2005).

[12] P. Drude, *Lehrbuch der Optik* (S. Hirzel, Leipzig, 1900).

[13] J. O. Hirschfelder, C. F. Curtiss, and R. B. Bird, *Molecular Theory of Gases and Liquids* (Wiley, New York, 1954).

[14] W. L. Bade and J. G. Kirkwood, J. Chem. Phys. **27**, 1284 (1957).

[15] A. A. Lucas, Phys. Rev. **176**, 1093 (1968).

[16] G. Lamoureux, A. D. MacKerell, and B. Roux, J. Chem. Phys. **119**, 5185 (2003).

[17] T. W. Whitfield and G. J. Martyna, J. Chem. Phys. **126**, 074104 (2007).

[18] A. Jones, A. Thompson, J. Crain, M. H. Muser, and G. J. Martyna, Phys. Rev. B **79**, 144119 (2009).

[19] A.G. Donchev, J. Chem. Phys. **125**, 074713 (2006).

[20] M. W. Cole and D. Velegol and H.-Y. Kim and A. A. Lucas, Mol. Simul. **35**, 849 (2009).

[21] Y. V. Shtogun and L. M. Woods, J. Phys. Chem. Lett. **1**, 1356 (2010).

[22] R.-F. Liu and J. G. Angyan and J. F. Dobson, J. Chem. Phys. **134**, 114106 (2011).

[23] A. Tkatchenko and R. A. DiStasio, Jr., and R. Car, and M. Scheffler, Phys. Rev. Lett. **108**, 236402 (2012).

[24] R. A. DiStasio, Jr. and O. A. von Lilienfeld and A. Tkatchenko, Proc. Natl. Acad. Sci. USA **109**, 14791 (2012).

[25] M. Sprik, M. L. Klein, and K. Watanabe, J. Phys. Chem. **94**, 6483 (1990).

[26] C. Burnham and S. Xantheas, J. Chem. Phys. **116**, 1479 (2002).

[27] R. Kumar, F. Wang, G. Jenness, and K. Jordan, J. Chem. Phys. **132**, 014309 (2010).

[28] Q. Smith, M. S. Gordon, and L. Slipchenko, J. Phys. Chem. A **115**, 4598 (2011).

[29] A. P. Bartok, M. C. Payne, R. Kondor, and G. Csanyi, Phys. Rev. Lett. **104**, 136403 (2010).

[30] S. Flügge, *Practical Quantum Mechanics*, Classics in Mathematics (Springer, New Jersey, USA, 1998), p. 166.

[31] A. J. Stone, *The Theory of Intermolecular Forces* (Clarendon Press, Oxford, 1996).

[32] A. D. Buckingham, *Advances in Chemical Physics: Intermolecular Forces*, Vol. 12 (John Wiley & Sons., New York, London, Sydney, 1967), Chap. 2, p. 107.

[33] See Supplemental Material at http://link.aps.org/supplemental/10.1103/PhysRevB.87.144103 for details of derivations.

[34] A. Jones, Ph.D. thesis, University of Edinburgh, Edinburgh, United Kingdom, 2010.

[35] R. Jastrow, Phys. Rev. **98**, 1479 (1958).

[36] J. Jenson and M. Gordon, Mol. Phys. **89**, 1313 (1996).

[37]V. Ovsiannikov, A. Guilyarovski, and O. Lopatko, Mol. Phys. **64**, 111 (1988).
[38]C. Millot and A. J. Stone, Mol. Phys. **77**, 439 (1992).
[39]B. M. Axilrod and E. Teller, J. Chem. Phys. **11**, 299 (1943).
[40]P. R. Fontana, Phys. Rev. **123**, 1865 (1961).
[41]J. Cao and B. J. Berne, J. Chem. Phys. **97**, 8628 (1992).
[42]E. A. Moelwyn-Hughes, *Physical Chemistry* (Pergamon Press, Oxford, 1961).
[43]G. D. Zeiss and W. J. Meath, Mol. Phys. **33**, 1155 (1977).
[44]K. T. Tang, Phys. Rev. **177**, 108 (1969).
[45]D. J. Margoliash, T. R. Proctor, G. D. Zeiss, and W. J. Meath, Mol. Phys. **35**, 747 (1978).
[46]T. D. Crawford and H. F. Schaefer, III, *Reviews in Computational Chemistry*, Vol. 14, edited by K. B. Lipkowitz and D. B. Boyd (Wiley, New York, 2000), p. 33.
[47]T. Helgaker, P. Jorgensen, and J. Olsen, *Molecular Electronic-Structure Theory* (Wiley, New York, 1999).
[48]E. Krotscheck, Phys. Rev. B **31**, 4267 (1985).
[49]E. Krotscheck, W. Kohn, and G.-X. Qian, Phys. Rev. B **32**, 5693 (1985).
[50]J. W. Clark, in *Progress in Nuclear and Particle Physics*, edited by D. H. Wilkinson (Pergamon, Oxford, 1979), Vol. 2, pp. 89.
[51]M. Georgiev, A. Gochev, and J. Singh, Internet Electron. J. Mol. Des. **4**, 765 (2005).
[52]T. W. Whitfield and G. J. Martyna, Chem. Phys. Lett. **424**, 409 (2006).
[53]J. A. Barker, R. A. Fisher, and R. O. Watts, Mol. Phys. **21**, 657 (1971).
[54]J. A. Barker, R. O. Watts, J. K. Lee, T. P. Schafer, and Y. T. Lee, J. Chem. Phys. **61**, 3081 (1974).
[55]B. Brunetti, R. Cambi, F. Pirani, F. Vecchiocattivi, and M. Tomassini, Chem. Phys. **42**, 397 (1979).
[56]J. F. Peng, P. Li, J. Ren, L. W. Qiao, and K. T. Tang, J. At. Mol. Sci. **2**, 289 (2011).
[57]R. A. Aziz, Chem. Phys. Lett. **28**, 47 (1974).
[58]R. A. Aziz, J. Chem. Phys. **99**, 4518 (1993).
[59]A. Stone, J. Chem. Theory Comput. **1**, 1128 (2005).
[60]M. Gordon, M. Freitag, P. Bandyopadhyay, J. Jensen, V. Kairys, and W. Stevens, J. Phys. Chem. A **105**, 293 (2001).
[61]R. P. Feynman, *Statistical Mechanics* (Westview Press, Boulder, Colorado, USA, 1998).
[62]U. Essmann, L. Perera, M. Berkowitz, T. Darden, H. Lee, and L. Pedersen, J. Chem. Phys. **103**, 8577 (1995).
[63]E. Pollock and J. Gloshi, Com. Phys. Comm. **95**, 93 (1996).
[64]M. Challacombe, C. White, and M. Head-Gordon, J. Chem. Phys. **107**, 10131 (1997).
[65]G. Martyna, A. Hughes, and M. Tuckerman, J. Chem. Phys. **110**, 3275 (1999).
[66]T. Kihara and S. Koba, J. Phys. Soc. Jpn. **7**, 348 (1952).
[67]C. Lin, F. H. Zong, and D. M. Ceperley, Phys. Rev. E **64**, 016702 (2001).
[68]F. Birch, Phys. Rev. **71**, 809 (1947).
[69]N. W. Ashcroft and N. D. Mermin, *Solid State Physics* (Holt, Rinehart and Winston, New York, 1976).
[70]G. K. Horton, Am. J. Phys. **36**, 93 (1968).
[71]C. P. Herrero, J. Phys.: Condens. Matter **15**, 475 (2003).